

On the space of $U(N)$ scattering amplitudes

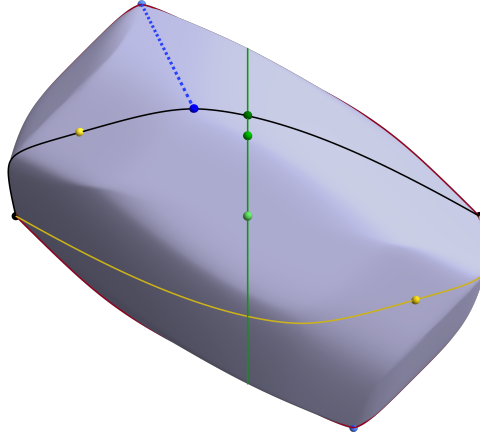
Lucía Córdova,^a Ricardo Rodrigues^b

^a*Department of Theoretical Physics, CERN, 1211 Meyrin, Switzerland*

^b*Centro de Física do Porto, Departamento de Física e Astronomia, Faculdade de Ciências da Universidade do Porto, Rua do Campo Alegre 687, 4169-007 Porto, Portugal*

E-mail: lucia.gomez.cordova@cern.ch, up201805119@edu.fc.up.pt

ABSTRACT: We investigate the space of massive two-dimensional theories with a global $U(N)$ symmetry and no bound states. Following S-matrix bootstrap principles, we establish rigorous bounds on the space of consistent $2 \rightarrow 2$ scattering amplitudes. The allowed regions exhibit rich geometric features with integrable models appearing at special points along the boundary. Generic extremal amplitudes display an infinite number of resonances and periodic behavior in energy, similar to previous studies with other group-like symmetries. Within the allowed space, we identify a subregion where the symmetry is enhanced to $O(2N)$, establishing a connection with earlier studies. We also revisit the classification of integrable solutions, identifying one that was previously overlooked in the literature. Finally, we examine the walking behavior of the central charge associated with several of these periodic amplitudes.



$U(2)$ monolith

Contents

1	Introduction	1
2	Preliminary notions	2
2.1	Numerical implementation	5
3	The space of allowed amplitudes	7
4	Discussion	14
A	Solutions to Yang-Baxter equations	19
A.1	General N	19
A.2	$N=2$	26
B	Integrable form factors and c-sum rule	29
C	Primal and dual codes	31
C.1	Primal	31
C.2	Dual	32

1 Introduction

The principles of analyticity, crossing symmetry, and unitarity of the S-matrix have proven extremely effective in constraining the space of consistent Quantum Field Theories. In contrast with the original S-matrix program of the 1960s, which aimed at finding a unique consistent S-matrix describing strong interactions, the modern S-matrix bootstrap [1, 2] approach has revealed a much richer landscape of possible theories. Particularly simple and instructive examples arise in two-dimensional gapped theories with a global symmetry [3–8], where the bootstrap constraints are already too complex to be solved analytically, making numerical analysis necessary.

An advantage of working in two spacetime dimensions is that one can make contact with integrable models, which offer the rare gift of exact non-perturbative amplitudes for interacting theories. Also, at a more technical level, the simplicity of two-dimensional kinematics allows for an in-depth analysis of extremal amplitudes –i.e. those saturating the bootstrap bounds– obtained numerically. In particular, these $2 \rightarrow 2$ amplitudes are parametrized by a small number (as many as irreps in the tensor product of the incoming particles) of functions of a single complex variable s , the center of mass energy, whose analytic structure in the complex plane can be thoroughly explored, even at large energies.

In this work, we explore the space of consistent two-dimensional massive theories with a global continuous symmetry $U(N)$. A previous study [9] established bounds on cubic

couplings in theories with bound states, where the $U(N)$ Gross-Neveu model appears as an extremal amplitude. However, general bootstrap bounds for theories without bound states, as well as a systematic understanding of the different classes of integrable solutions within the space of amplitudes, remained unexplored. We address this gap by deriving rigorous bounds on the possible values of amplitudes at the crossing-symmetric point, using the dual approach formulated in [5].

Our results show integrable physical theories, such as the integrable “massive” CP^{N-1} model studied in [10], the $O(2N)$ non-linear sigma model (NLSM), and free theories, all sitting at vertices of the allowed space. The remaining classes of integrable solutions with periodic behavior in energy, one of which was previously overlooked in the literature, also appear at the boundary of this space. We also find that the rest of extremal amplitudes generically have an infinite number of resonances and exhibit periodic behavior in real rapidity.

The paper is organized as follows: in section 2 we review the necessary group theory concepts to define the amplitudes under consideration, as well as the physical principles used to bootstrap them. We also explain the numerical implementation used to derive bounds. In section 3 we present our results, showing various subsections of the space of allowed $U(N)$ amplitudes, along with a full classification of integrable amplitudes that live in this space. We also discuss various features of the extremal amplitudes. Finally in section 4 we examine the walking behavior of the UV central charge for periodic amplitudes, hinting to the presence of complex conformal theories.

Several appendices complement this work: in appendix A we present a thorough review of the classification of integrable amplitudes, in appendix B we give more details on the integrable form factors used to compute the central charges, and in appendix C we provide examples of the dual and primal bootstrap codes used to derive numerical bounds.

2 Preliminary notions

In this section we will address the structure of the S-matrix for the scattering of $U(N)$ charged particles of mass m and the conditions which constrain it. In particular, we focus on two body scattering of particles transforming in the fundamental representation.

Given that the symmetry group $U(N)$ is complex, this implies that we will have particles, transforming under an irreducible representation \mathcal{R} , as well as antiparticles transforming under the corresponding complex conjugate irrep $\overline{\mathcal{R}}$. As such, there are two physically distinct scenarios: particle-particle and particle-antiparticle scattering. For these two cases the two-dimensional S-matrix can be written as:

$$\langle P_{\bar{\delta}}(p_4)P_{\bar{\gamma}}(p_3) | \mathcal{S} | P_{\alpha}(p_1)P_{\beta}(p_2) \rangle = S_{\alpha\beta}^{\bar{\delta}\bar{\gamma}}(\theta) [\delta_{k_1,k_3}\delta_{k_2,k_4} \pm \delta_{k_1,k_4}\delta_{k_2,k_3}] , \quad (2.1)$$

$$\langle A_{\delta}(p_4)P_{\bar{\gamma}}(p_3) | \mathcal{S} | P_{\alpha}(p_1)A_{\bar{\beta}}(p_2) \rangle = F_{\alpha\bar{\beta}}^{\delta\bar{\gamma}}(\theta) \delta_{k_1,k_3}\delta_{k_2,k_4} + B_{\alpha\bar{\beta}}^{\bar{\gamma}\delta}(\theta) \delta_{k_1,k_4}\delta_{k_2,k_3} , \quad (2.2)$$

where P_{α} , $P_{\bar{\alpha}}$ denote respectively ingoing and outgoing particle states whereas $A_{\bar{\beta}}$ and A_{β} designate ingoing and outgoing antiparticle states, and $p_i^{\mu} = (E_i, k_i)$. Furthermore, the rapidity variable θ is related with the usual Mandelstam invariant $s = (p_1 + p_2)^2$ by

$s = 4m^2 \cosh^2(\theta/2)$. In the first equation the \pm sign accounts for the bosonic (+) or fermionic (-) nature of the particles. Moreover, $F_{\alpha\bar{\beta}}^{\delta\bar{\gamma}}(\theta)$ denotes the forward amplitude whereas $B_{\alpha\bar{\beta}}^{\bar{\gamma}\delta}(\theta)$ is the backward amplitude. All three functions in the above equations are related to each other by crossing symmetry

$$S_{\alpha\bar{\beta}}^{\bar{\delta}\bar{\gamma}}(i\pi - \theta) = F_{\alpha\bar{\delta}}^{\beta\bar{\gamma}}(\theta) \quad , \quad B_{\alpha\bar{\beta}}^{\bar{\gamma}\delta}(i\pi - \theta) = B_{\delta\bar{\beta}}^{\bar{\gamma}\alpha}(\theta) \quad , \quad (2.3)$$

which translates the fact that by swapping ingoing and outgoing particles in one scattering process we can get a different one.

As found in [11] we can write the functions S , F and B in terms of $U(N)$ invariant amplitudes

$$S_{\alpha\bar{\beta}}^{\bar{\delta}\bar{\gamma}}(\theta) = \begin{array}{c} \bar{\delta} \quad \bar{\gamma} \\ \diagdown \quad \diagup \\ \text{S} \\ \diagup \quad \diagdown \\ \alpha \quad \beta \end{array} = u_1(\theta) \begin{array}{c} \bar{\delta} \quad \bar{\gamma} \\ \diagdown \quad \diagup \\ \alpha \quad \beta \end{array} + u_2(\theta) \begin{array}{c} \bar{\delta} \quad \bar{\gamma} \\ \curvearrowright \quad \curvearrowleft \\ \alpha \quad \beta \end{array} \quad , \quad (2.4)$$

$$F_{\alpha\bar{\beta}}^{\delta\bar{\gamma}}(\theta) = \begin{array}{c} \delta \quad \bar{\gamma} \\ \diagdown \quad \diagup \\ \text{F} \\ \diagup \quad \diagdown \\ \alpha \quad \bar{\beta} \end{array} = t_1(\theta) \begin{array}{c} \delta \quad \bar{\gamma} \\ \diagdown \quad \diagup \\ \alpha \quad \bar{\beta} \end{array} + t_2(\theta) \begin{array}{c} \delta \quad \bar{\gamma} \\ \curvearrowright \quad \curvearrowleft \\ \alpha \quad \bar{\beta} \end{array} \quad , \quad (2.5)$$

$$B_{\alpha\bar{\beta}}^{\bar{\gamma}\delta}(\theta) = \begin{array}{c} \bar{\gamma} \quad \delta \\ \diagdown \quad \diagup \\ \text{B} \\ \diagup \quad \diagdown \\ \alpha \quad \bar{\beta} \end{array} = r_1(\theta) \begin{array}{c} \bar{\gamma} \quad \delta \\ \curvearrowright \quad \curvearrowleft \\ \alpha \quad \bar{\beta} \end{array} + r_2(\theta) \begin{array}{c} \bar{\gamma} \quad \delta \\ \curvearrowleft \quad \curvearrowright \\ \alpha \quad \bar{\beta} \end{array} \quad , \quad (2.6)$$

where each diagram represents the product of two Kronecker deltas.

In this basis the crossing relations are straightforward. Indeed, by looking at the pictorial representations it is easy to see that some of diagrams are related by a rotation of 90° . Since this rotation amounts to sending $\theta \rightarrow i\pi - \theta$, it easily follows that crossing translates into

$$u_1(\theta) = t_1(i\pi - \theta) \quad , \quad u_2(\theta) = t_2(i\pi - \theta) \quad , \quad r_1(\theta) = r_2(i\pi - \theta) \quad . \quad (2.7)$$

Alternatively the S-matrix can be decomposed in terms of the representations of $U(N)$ that appear in the product of the fundamental representation N with itself or with its complex conjugate \bar{N} :

$$N \otimes N = \frac{N(N+1)}{2} \oplus \frac{N(N-1)}{2} \quad , \quad N \otimes \bar{N} = 1 \oplus (N^2 - 1) \quad , \quad (2.8)$$

where on the left equation the representations correspond to the symmetric and antisymmetric representations respectively, whereas on the right one we encounter the singlet and the adjoint representations. In this basis we have

$$S = S_{\text{sym}}(\theta) \mathbb{T}_{\text{sym}} + S_{\text{anti}}(\theta) \mathbb{T}_{\text{anti}} \quad , \quad (2.9)$$

$$F^+ \equiv F + B = S_{\text{sing}}^+(\theta) \mathbb{T}_{\text{sing}} + S_{\text{adj}}^+(\theta) \mathbb{T}_{\text{adj}} \quad , \quad (2.10)$$

$$F^- \equiv F - B = S_{\text{sing}}^-(\theta) \mathbb{T}_{\text{sing}} + S_{\text{adj}}^-(\theta) \mathbb{T}_{\text{adj}} \quad , \quad (2.11)$$

where we have defined F^\pm as in [9], with \pm denoting the parity, and with the representations' structures given by

$$(\mathbb{T}_{\text{sym}})_{\alpha\beta}^{\bar{\delta}\bar{\gamma}} = \frac{1}{2} \left(\delta_{\alpha}^{\bar{\gamma}} \delta_{\beta}^{\bar{\delta}} + \delta_{\alpha}^{\bar{\delta}} \delta_{\beta}^{\bar{\gamma}} \right) , \quad (\mathbb{T}_{\text{anti}})_{\alpha\beta}^{\bar{\delta}\bar{\gamma}} = \frac{1}{2} \left(\delta_{\alpha}^{\bar{\gamma}} \delta_{\beta}^{\bar{\delta}} - \delta_{\alpha}^{\bar{\delta}} \delta_{\beta}^{\bar{\gamma}} \right) , \quad (2.12)$$

$$(\mathbb{T}_{\text{sing}})_{\alpha\beta}^{\delta\bar{\gamma}} = \frac{1}{N} \delta_{\alpha\bar{\beta}} \delta^{\delta\bar{\gamma}} , \quad (\mathbb{T}_{\text{adj}})_{\alpha\beta}^{\delta\bar{\gamma}} = \delta_{\alpha}^{\bar{\gamma}} \delta_{\beta}^{\delta} - \frac{1}{N} \delta_{\alpha\bar{\beta}} \delta^{\delta\bar{\gamma}} . \quad (2.13)$$

The two basis we introduced are related in the following way:

$$\begin{aligned} S_{\text{sym}} &= u_1 + u_2 , & S_{\text{anti}} &= u_1 - u_2 , \\ S_{\text{sing}\pm} &= t_1 \pm r_1 + N(t_2 \pm r_2) , & S_{\text{adj}\pm} &= t_1 \pm r_1 . \end{aligned} \quad (2.14)$$

Using this map it is possible to reexpress the crossing conditions in (2.7) in terms of the functions S_a ($a \in \text{sing } \pm, \text{adj } \pm, \text{sym}, \text{anti}$) as

$$S_a(i\pi - \theta) = C_{ab} S_b(\theta) . \quad (2.15)$$

with

$$\mathbf{S}(\theta) \equiv \begin{pmatrix} S_{\text{sing}+}(\theta) \\ S_{\text{adj}+}(\theta) \\ S_{\text{sing}-}(\theta) \\ S_{\text{adj}-}(\theta) \\ S_{\text{sym}}(\theta) \\ S_{\text{anti}}(\theta) \end{pmatrix} , \quad (2.16)$$

and where the crossing matrix C_{ab} is given by

$$C_{ab} \equiv \begin{pmatrix} \frac{1}{2N} & \frac{N^2-1}{2N} & -\frac{1}{2N} & \frac{1-N^2}{2N} & \frac{1+N}{2} & \frac{1-N}{2} \\ \frac{1}{2N} & -\frac{1}{2N} & -\frac{1}{2N} & \frac{1}{2N} & \frac{1}{2} & \frac{1}{2} \\ -\frac{1}{2N} & \frac{1-N^2}{2N} & \frac{1}{2N} & \frac{N^2-1}{2N} & \frac{1+N}{2} & \frac{1-N}{2} \\ -\frac{1}{2N} & \frac{1}{2N} & \frac{1}{2N} & -\frac{1}{2N} & \frac{1}{2} & \frac{1}{2} \\ \frac{1}{2N} & \frac{N-1}{2N} & \frac{1}{2N} & \frac{N-1}{2N} & 0 & 0 \\ -\frac{1}{2N} & \frac{1+N}{2N} & -\frac{1}{2N} & \frac{1+N}{2N} & 0 & 0 \end{pmatrix} , \quad (2.17)$$

such that it satisfies $C^2 = \mathbb{1}$.

In the basis of (2.9), (2.10) and (2.11), the unitarity conditions for the S-matrix translate into

$$|S_a(\theta)|^2 \leq 1 \quad (a = \text{sing } \pm, \text{adj } \pm, \text{sym}, \text{anti}) , \quad (2.18)$$

for $\theta \geq 0$ in the real axis, i.e. $s \geq 4m^2$. These are somewhat simpler than if expressed in the u_i, t_i, r_i ($i = 1, 2$) basis, which can be easily obtained from the above inequalities by making use the map (2.14).

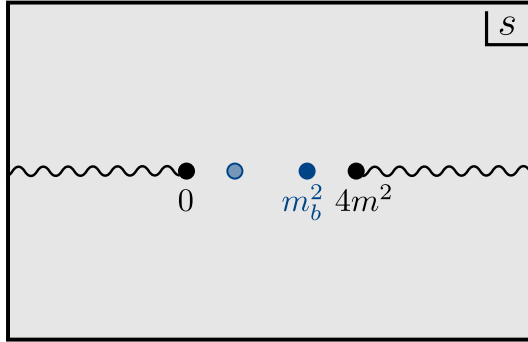


Figure 1: Analytic structure of the S-matrix function $S(s)$ in the complex plane $s \in \mathbb{C}$. Poles are connected with the existence of bound states whereas branch cuts represent multi-particle thresholds.

2.1 Numerical implementation

We shall now say a few words about how the space of the allowed amplitudes is mapped in practice. The reader familiar with S-matrix bootstrap can safely skip this section and proceed to the next one.

Regardless of the approach one follows, when bootstrapping the S-matrix we must always bear in mind and impose the three consistency conditions previously mentioned:

- We assume that the S-matrix $\mathbf{S}(s)$ is an analytic function in the s complex plane apart from possible poles representing bound states and branch cuts for intermediate multi-particle states, as depicted in figure 1. In our case we assume no bound states in the spectrum such that we should only have branch cuts for $s \geq 4m^2$ and $s \leq 0$, where the latter concerns the t -channel;
- Moreover, we also impose that the amplitude is crossing symmetric, as the s-and t-channel processes are boundary values of the same analytic function. For the simplest case of $2 \rightarrow 2$ scattering of identical particles this translates into $S(s) = S(t = 4m^2 - s)$. In our case where we have a certain global symmetry and consequently a function for each representation of the group, this condition is slightly more convoluted (2.15);
- Lastly, the full S-matrix must also satisfy the unitarity condition, namely that the S-matrix operator is an unitary operator $\mathcal{S}\mathcal{S}^\dagger = \mathbb{1}$. From a quantum mechanics perspective this is simply the statement of probability conservation. For the case mentioned before, specifically the scattering of identical particles with no global symmetry, the unitarity condition translates to: $|S(s)|^2 \leq 1$ for $s \geq 4m^2$. Seeing as in here we have several functions for each representation, each of these must satisfy a similar unitarity condition as expressed in (2.18);

Based in these conditions, the numerical bootstrap can be carried out in two different ways.

In the primal approach, put forward in [2], we start by constructing an ansatz for the S-matrix that automatically satisfies both crossing and analyticity. One such possible

choice is

$$\mathbf{S}(s) = \mathbf{S}_0 + \sum_{k=1}^{\infty} \left[\mathbf{S}_k \rho_{2m^2}^k(s) + \mathcal{C} \cdot \mathbf{S}_k \rho_{2m^2}^k(4m^2 - s) \right], \quad (2.19)$$

where

$$\mathbf{S}_n = \begin{pmatrix} \text{sing}_n^+ \\ \text{adj}_n^+ \\ \text{sing}_n^- \\ \text{adj}_n^- \\ \text{sym}_n \\ \text{anti}_n \end{pmatrix}, \quad n \in \mathbb{N}_0 \quad (2.20)$$

is a vector of coefficients for this Taylor-like expansion of each one of the components of the S-matrix, and the variable

$$\rho_{s_0}(s) = \frac{\sqrt{4m^2 - s_0} - \sqrt{4m^2 - s}}{\sqrt{4m^2 - s_0} + \sqrt{4m^2 - s}}, \quad (2.21)$$

maps the right half plane of $s \in \mathbb{C}$ into the unit disk, where in particular s_0 gets mapped to its origin, see for example [12, 13]. Crucially, this variable takes care of analyticity as the $s \geq 4m^2$ branch cut is mapped to the boundary of the disk. As for crossing, it is easy to see from (2.19), which was written purposefully in a crossing symmetric way, that it satisfies (2.15). After we construct the ansatz for the S-matrix we choose a given functional $\mathcal{F}[\mathbf{S}(s)]$ which we want to maximize, while simultaneously imposing the unitarity condition. This fixes the coefficients in (2.19) and provides (an approximation) of a consistent scattering amplitude. In practice, unitarity is imposed by evaluating our ansatz at several points s_i ($i = 1, \dots, N_{\text{grid}}$) in the physical region $s \geq 4m^2$, and demanding that in each of these $|S_a(s_i)|^2 \leq 1$ ($a = \text{sing } \pm, \text{adj } \pm, \text{sym}, \text{anti}$) is satisfied. As for the functionals, some of the usual choices for these correspond to: $\mathcal{F}[\mathbf{S}(s)] = \mathbf{S}(s_*)$ for $0 < s_* < 4m^2$, $\mathcal{F}[\mathbf{S}(s)] = \text{Res}_{s=m_b^2} \mathbf{S}(s)$ where m_b is some bound state mass, between others. By optimizing these functionals we bound the space of allowed amplitudes as desired. The benefit of the primal approach is that by the end of the process we end up with an explicit expression of the S-matrix, which in spite of being an approximation, is good enough to allow us to study some of its characteristics. However, there is also a downside to this approach, which is that the bounds are not rigorous and their values depend on the number of parameters we include in the ansatz.

On the other hand we have the dual approach first introduced in [5] and later extended to different settings in [14–20], which not only places rigorous bounds as it is also faster than the primal one. In this method we first optimize a dual functional $\mathcal{F}_d(\mathbf{K}(s))$ in terms of dual functions $\mathbf{K}(s)$, which serve as Lagrange multipliers for the S-matrix constraints. To give a concrete example, if we want to put bounds on $S(2m^2)$ the dual function has the

following form

$$\mathbf{K}(s) = \frac{1}{(s - 2m^2) \sqrt{s(s - 4m^2)}} \left\{ \sum_{i=1}^3 a_i \mathbf{v}_i + \sum_{j=1}^{\infty} \left[\mathbf{K}_j \rho_{2m^2}^j(s) + \mathcal{C}^T \cdot \mathbf{K}_j \rho_{2m^2}^j(4m^2 - s) \right] \right\}, \quad (2.22)$$

where the coefficients a_i are to be fixed by the optimization procedure, \mathbf{v}_i are eigenvectors of \mathcal{C}^T of eigenvalue 1 and \mathbf{K}_j are vectors of coefficients similar to (2.20). The initial prefactor is crucial in order to guarantee that we are exploring the space of amplitudes at the crossing symmetric point $s = 2m^2$, and at the same time takes care of the desired decay rate as $s \rightarrow \infty$. The function $\mathbf{K}(s)$ also satisfies an anti-crossing condition with respect to the transverse crossing matrix \mathcal{C}^T , i.e. $\mathbf{K}(4m^2 - s) = -\mathcal{C}^T \cdot \mathbf{K}(s)$. This can be easily be seen to hold with the above ansatz. The dual functional $\mathcal{F}_d[\mathbf{K}(s)]$ is given by

$$\mathcal{F}_d[\mathbf{K}(s)] = \frac{2}{\pi} \int_{4m^2}^{\infty} ds \sum_a |K_a(s)|, \quad (2.23)$$

where the sum is over the components of $\mathbf{K}(s)$ and where the integration can be numerically achieved with the Chebyshev method, for example. It is also important that each $K_a(s)$ decays at least like $s^{-3/2}$ in order for the integral to converge. Finally, we minimize this functional which by construction satisfies

$$\max_{\{\mathbf{S}\}} \mathcal{F}[\mathbf{S}(s)] \leq \min_{\{\mathbf{K}\}} \mathcal{F}_d[\mathbf{K}(s)], \quad (2.24)$$

implying that we are always approaching the optimal bound from above. One of the reasons why this method is faster when compared with the primal one is that we do not have to impose the unitarity constraints while minimizing the dual functional.

In this work we we used both methods to insure optimality of our bounds. The `Mathematica` codes for the two approaches can be found in appendix C. Finally, we mention that for the minimization / maximization of functionals, we have used the optimization solver library `MOSEK` [21], which significantly reduces the required time compared to the built-in methods of `Mathematica`.

3 The space of allowed amplitudes

In this section we present two- and three-dimensional subsections of the allowed space of two-body amplitudes with global $U(N)$ symmetry. These sections are obtained by placing numerical bounds on the functions t_1, t_2, r_1 (see equations 2.4-2.6) at the crossing symmetric point $\theta = i\pi/2$ ($s = 2m^2$). Figures 2-5 show these spaces for $N = 2$ and $N = 7$. The bootstrap implementation utilized to generate these plots is explained in 2.1 and appendix C.

The first thing to note from the above figures is that the space of allowed amplitudes is convex. This follows from various properties of the amplitudes: the unitarity condition in physical kinematics, analyticity inside the physical sheet and boundedness at the left hand cut due to crossing.

Let us now discuss the symmetries of this allowed space. That is, given an extremal amplitude $S_a(\theta)$ saturating the bootstrap constraints, we want to understand which simple maps lead us to another point at the boundary. Note first that we are allowed to simultaneously change the overall sign of the amplitudes $S_a \rightarrow -S_a$ without spoiling any of the analyticity, crossing and unitarity conditions.¹ Other symmetries come from flipping the sign of only some of the u_i, t_i, r_i components. For instance, sending $r_{1,2} \rightarrow -r_{1,2}$ ² simply flips the parity even and odd sectors $S_{\text{sing } \pm} \rightarrow S_{\text{sing } \mp}, S_{\text{adj } \pm} \rightarrow S_{\text{adj } \mp}$. Finally we can also make the following simultaneous change of signs $u_{1,2} \rightarrow -u_{1,2}, t_{1,2} \rightarrow -t_{1,2}$, which can be thought of as a composition of the latter two transformations.

The spaces of allowed amplitudes presented³ in figures 2 and 4 have various geometric features such as sharp edges and vertices. We have identified various integrable points (class I-VII in figures) and constant solutions (const. 1 and 2) for which we can write exact non-perturbative expressions which we review below.

Integrable amplitudes These describe theories where there is an infinite number of conserved charges which imply the absence of particle production and factorized scattering. The latter condition is imposed through the Yang-Baxter equations, which tell us we can factorize $3 \rightarrow 3$ scattering into different sequences of $2 \rightarrow 2$ processes:

$$(3.1)$$

When the scattered particles are charged under a global symmetry, these equations are highly constraining and their solutions can be classified. For theories with $U(N)$ symmetry this classification was first performed in [11]. In table 1 we present a revised version of the different classes of integrable amplitudes.⁴ In appendix A we review how the different classes arise when solving Yang-Baxter equations. The building block for these amplitudes is the function:

$$f_\lambda(\theta) = \frac{\Gamma(\frac{1}{2} + \frac{\theta}{2\pi i})\Gamma(\frac{1}{2} + \frac{\lambda}{2} - \frac{\theta}{2\pi i})}{\Gamma(\frac{1}{2} - \frac{\theta}{2\pi i})\Gamma(\frac{1}{2} + \frac{\lambda}{2} + \frac{\theta}{2\pi i})}, \quad (3.2)$$

¹This is only true if there are no bound states in the theory, as the residue at the bound state pole should have a definite sign.

²Both components r_1 and r_2 should be transformed simultaneously due to crossing symmetry.

³Both figures 2 and 4 were obtained using the dual approach functions in appendix C with $nmax = 10$, $nintpts = 30$, $precision = 100$ and approximately 120,000 different angles to scan the space.

⁴The classification proposed in table 1 of [11] has some inaccuracies in the expressions for classes V and VI and misses two other classes: an extra solution with a free parameter when $N = 2$ discussed in subsequent works [22, 23] and what we call class VII in table 1, which to our knowledge has not appeared in the literature before.

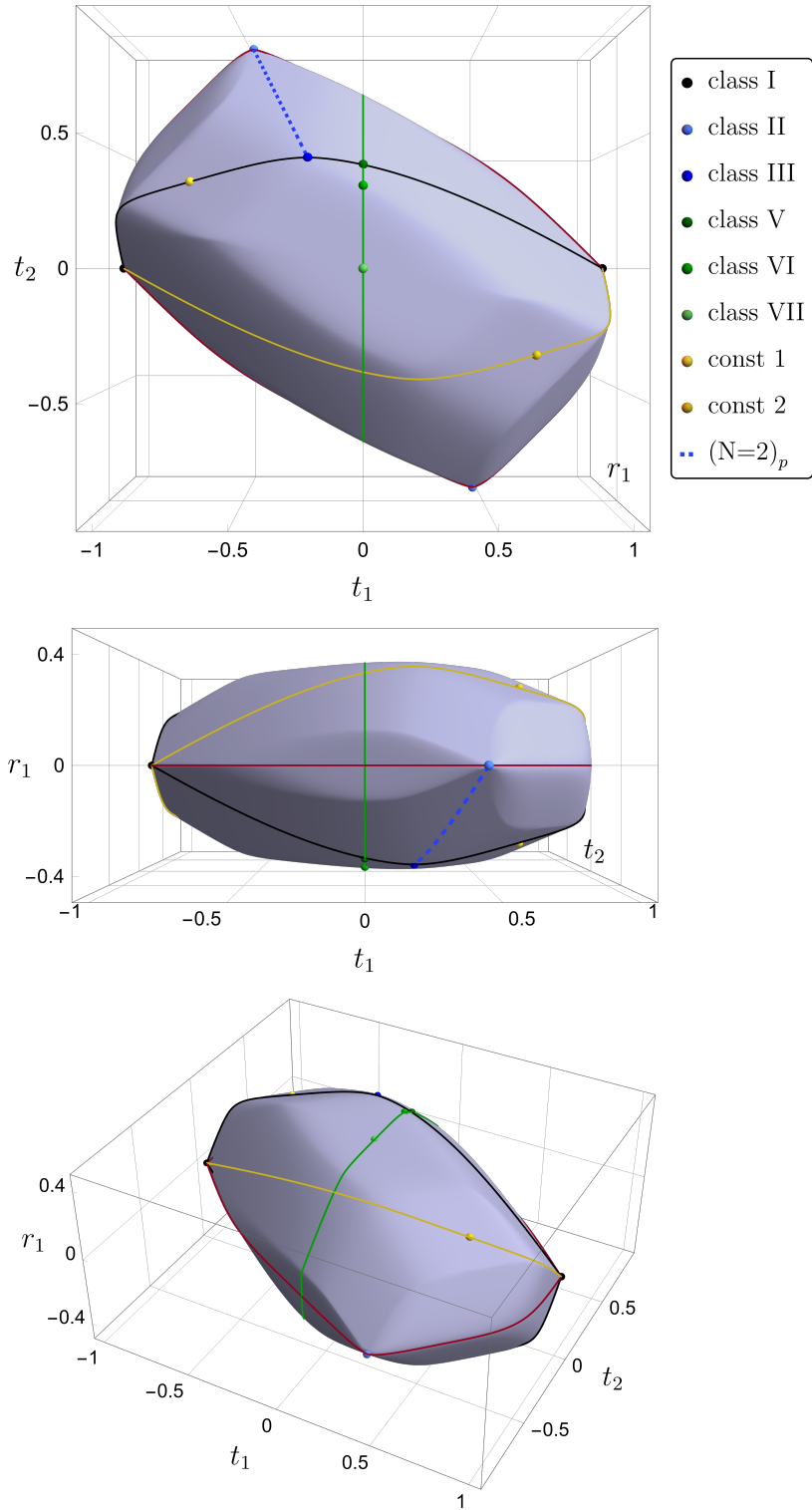


Figure 2: $U(2)$ monolith giving the space of allowed amplitudes parametrized by $\{t_1, t_2, r_1\}$ in (2.4-2.6) at the crossing symmetric point $\theta = i\pi/2$. Integrable (table 1) and constant solutions (3.3) situated at the boundary are highlighted.

Class	parameter	$t_1(\theta)$	$t_2(\theta)$	$r_1(\theta)$
I		1	0	0
II	$\lambda = \frac{2}{N}$	$f_\lambda(\theta)$	$-\frac{i\pi\lambda}{\tilde{\theta}} t_1(\theta)$	0
III	$\lambda = \frac{1}{N-1}$	$f_\lambda(\theta)f_\lambda(\tilde{\theta})$	$-\frac{i\pi\lambda}{\tilde{\theta}} t_1(\theta)$	$-\frac{i\pi\lambda}{\theta} t_1(\theta)$
IV	$\lambda = \frac{1}{N+1}$	$f_\lambda(\theta)f_\lambda(\tilde{\theta}) i \operatorname{th}\left(\frac{\theta}{2} - \frac{i\pi}{4}\right)$	$-\frac{i\pi\lambda}{\tilde{\theta}} t_1(\theta)$	$\frac{i\pi\lambda}{\theta} t_1(\theta)$
V	$\operatorname{ch}(\pi\mu) = N$	0	$\frac{\sin \mu\theta}{\sin \mu\tilde{\theta}} r_1(\theta)$	$\prod_{k \in \mathbb{Z}} \frac{f_{1-ik/\mu}(\theta)}{f_{ik/\mu}(\theta)}$
VI	$e^{\pi\mu} = N$	0	$e^{i\mu\tilde{\theta}} \frac{\sin \mu\theta}{\sin \mu\tilde{\theta}} r_1(\theta)$	$\prod_{k \in \mathbb{Z}} \frac{f_{1-ik/\mu}(\theta)}{f_{ik/\mu}(\theta)}$
VII	$\operatorname{ch}(\pi\mu) = \frac{N}{2}$	0	0	$\prod_{k \in \mathbb{Z}} \frac{f_{1-ik/\mu}(\theta)}{f_{ik/\mu}(\theta)}$
$(N=2)_p$	$p \in [1, \infty)$	$\frac{\operatorname{sh}(\theta/p)}{\operatorname{sh}(\tilde{\theta}/p)} f_1(\theta) \xi_p(\theta)$	$-\frac{i\pi}{\tilde{\theta}} t_1(\theta)$	$-\frac{\operatorname{sh}(i\pi/p)}{\operatorname{sh}(\theta/p)} t_1(\theta)$

Table 1: Classification of integrable amplitudes with $U(N)$ global symmetry. Classes I-VII give solutions to Yang-Baxter equations without free parameters valid for any N , whereas the last entry is an extra family of solutions arising when $N = 2$. The functions $f_\lambda(\theta)$ and $\xi_p(\theta)$ are respectively defined in (3.2) and (A.76) and we have used the shorthand notations: $\tilde{\theta} = i\pi - \theta$, $\operatorname{sh}=\sinh$, $\operatorname{ch}=\cosh$ and $\operatorname{th}=\tanh$. These amplitudes are the “minimal” integrable amplitudes without bound state poles.

which already captures some of the unitarity and crossing requirements.⁵

Now let us discuss the models described by the amplitudes in table 1. Free theories are described by Class I; class II solutions appear in the theories discussed in [10], sometimes called massive CP^{N-1} models,⁶ and class III coincides with the amplitudes of $O(2N)$ non-linear sigma model [29]. Classes V-VII are solutions to Yang-Baxter equations which are periodic in the real θ direction, with period $2\pi/\mu$. To the best of our knowledge, no precise identification of physical models has been made for the latter amplitudes (see section 4 for a discussion on possible connection to loop models and complex conformal theories). Finally, the free parameter solution for $N = 2$ describes the deformation of the $O(4)$ non-linear sigma model in [22, 23].

Except for class IV for which –because of the $\tanh\left(\frac{\theta-i\pi/2}{2}\right)$ factor in $t_1(\theta)$ – amplitudes

⁵By this we mean that starting from a pole in the complex plane, its images under crossing $\theta \rightarrow i\pi - \theta$ and unitarity $\theta \rightarrow -\theta$ naturally lead to the ratio of gamma functions in (3.2).

⁶There is a rich history behind these models, see e.g. [24–28], which can be seen as the CP^{N-1} model coupled to fermions or as a one parameter deformations of the $O(2N)$ non-linear sigma models. For $N > 2$ they are integrable only for special tuning of the parameters [10].

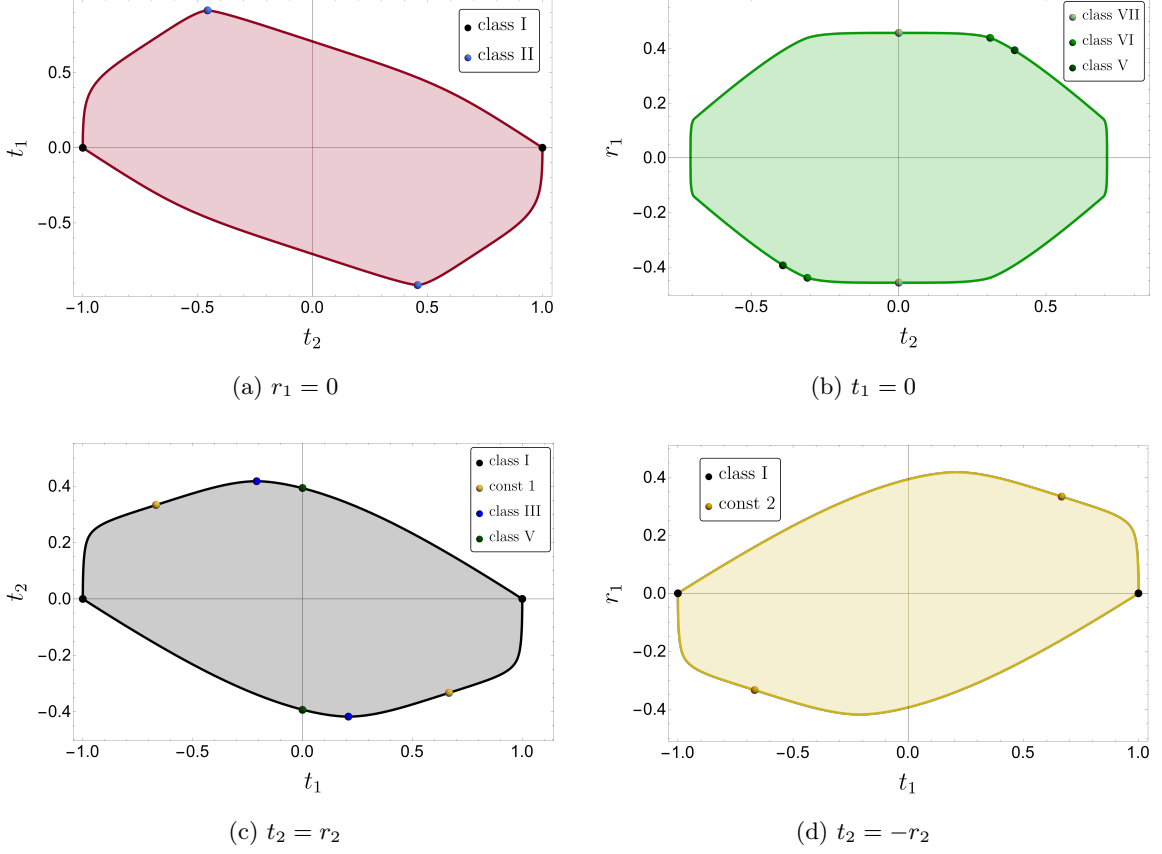


Figure 3: Sections of the $U(2)$ monolith (see solid lines in figure 2), obtained with the dual code in appendix C using $n_{max} = 30$, $n_{intpts} = 90$, $precision = 100$ and ~ 1000 angles.

vanish at the crossing symmetric point, all of the integrable amplitudes in table 1 appear at the boundary of the monolith, i.e. they are *extremal* amplitudes. These points are highlighted in different colors in figures 2-5. Note that the transformation $S_a \rightarrow -S_a$ gives an equally good solution to the Yang Baxter equations, so that for each class we have two integrable points on the monolith. Moreover, classes I-III are vertices of the allowed regions for any N and class VI for $N = 2$.

Constant solutions Another set of extremal amplitudes for which we have exact solutions is given by constant amplitudes which, in contrast to free theory, do not saturate the unitarity constraint in all channels. In the notation of (2.16) we have

$$\mathbf{S}_{\pm \text{const 1}} = \pm \begin{pmatrix} 1 \\ \frac{1-N}{1+N} \\ -1 \\ -1 \\ \frac{1-N}{1+N} \\ -1 \end{pmatrix}, \quad \mathbf{S}_{\pm \text{const 2}} = \pm \begin{pmatrix} -1 \\ -1 \\ 1 \\ \frac{1-N}{1+N} \\ \frac{1-N}{1+N} \\ -1 \end{pmatrix}, \quad (3.3)$$

where the two solutions are related by the exchange of parity even and odd sectors. This type of solutions were called yellow points in [5] and are highlighted in different shades of that color in figures 2-5. Since they are solutions to both the simplest primal and dual bootstrap problems, that is giving $S_a = c_a$ and $K_a(\theta) = in_a/\cosh\theta$ as ansatz, these points sit in the middle of flat faces (see e.g. figure 4 in [5]).

Unitarity saturation We observe that all extremal amplitudes –except for the constant solutions (3.3)– saturate the unitarity constraint $|S_a(\theta \geq 0)|^2 \leq 1$. This is a common (albeit unwelcome) feature in S-matrix bootstrap explorations, as non-integrable theories should allow for multiparticle processes $S_{2 \rightarrow n > 2} \neq 0$. Indeed, in the absence of multiparticle data the algorithm that maximizes a given functional will produce amplitudes which are as large as possible at the boundary of the physical sheet. Nevertheless, low energy observables such as the bounds discussed here are virtually unaffected by possible particle production at higher energies. Our claim is that the amplitudes found here still provide a good low-energy approximation to physical ones.⁷

Sections and global symmetry In figures 3 and 5 we show different sections of the $U(N)$ monoliths. The first one labeled by (a) is the section where $r_{1,2}(i\pi/2) = 0$. What we see is that the extremal amplitudes obey $r_{1,2}(\theta) = 0$ for all energies, so that there is no backward scattering. There are two (four, taking into account the $S_a \rightarrow -S_a$ symmetry) vertices corresponding to integrable theories: class I, i.e. free theory, and class II. In section (b) we find that extremal amplitudes obey $t_1(\theta) = u_1(\theta) = 0$, so that the transmission part of the amplitude vanishes. It is in this section that we find the periodic integrable amplitudes (classes V-VII) and class VI sits at a vertex for $N = 2$. The extremal amplitudes in section (c) satisfy $t_2(\theta) = r_2(\theta)$ and $u_1(\theta) = t_1(\theta)$ (as well as $u_2(\theta) = r_1(\theta)$ from crossing). What this means is that these amplitudes do not differentiate particles from antiparticles and the global symmetry is enhanced to $O(2N)$. The section indeed reproduces the results of [5], where the exact amplitudes highlighted with points are: free theory, the first constant solution in (3.3), the $O(2N)$ non-linear sigma model and the $O(2N)$ “periodic Yang-Baxter”. Finally section (d) shows the same amplitudes as in (c) except for the change of sign: $r_{1,2} \rightarrow -r_{1,2}$, which for non-trivial amplitudes spoils integrability.

Resonances and periodicity Similar to the space of $O(N)$ amplitudes in [4, 5], the extremal amplitudes generically exhibit an infinite number of resonances in the physical Riemann sheet. These can be detected as zeros in the complex rapidity plane with $0 \leq \text{Im}(\theta) \leq \pi$. An example is presented in figure 6 for a point on the boundary of the $U(7)$ monolith, close to the constant 1 solution. We also observe that these resonances arrange themselves in a way such that the amplitude is periodic. We show this periodic behavior in physical kinematics in figure 7 for an extremal amplitude with $N = 1000$.⁸ While this periodicity in (a parametrization of the) energy might seem strange from a physical point of view, it

⁷For a discussion on how adding an arbitrary function for particle production at a given energy threshold modifies both the bounds and the amplitudes’ analytic structure see e.g [4, 30].

⁸The periods generically decrease with N , so we chose a large number of flavors to show the periodicity up to “low” energies $\theta \approx 8$ ($s \approx 3000m^2$) where the numerical amplitudes are more reliable.

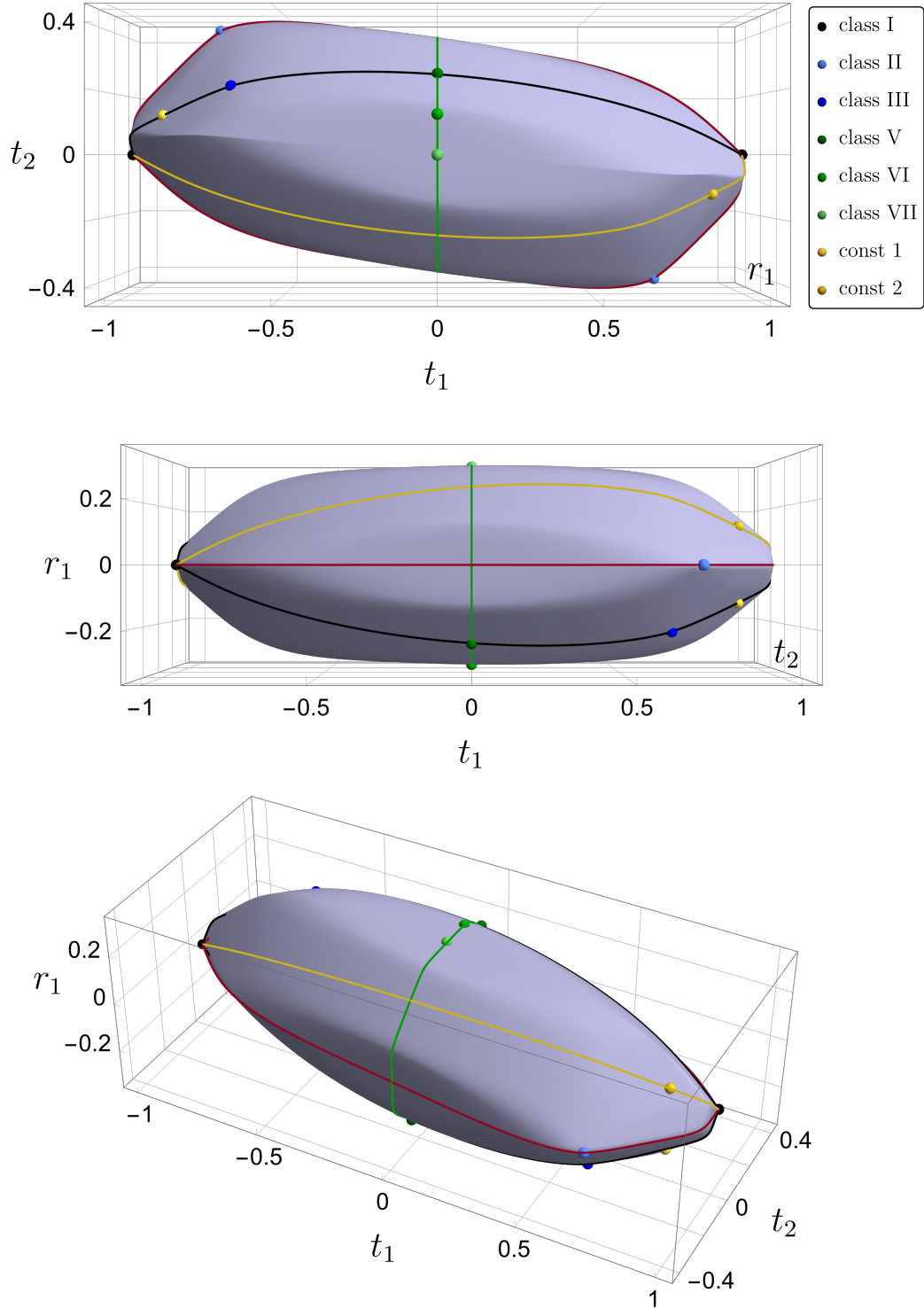


Figure 4: $U(7)$ monolith depicting the allowed space of the amplitudes parametrized by $\{t_1, t_2, r_1\}$ (see equations 2.4-2.6) at the crossing symmetric point $\theta = i\pi/2$. Points at the boundary with exact integrable (table 1) and constant (3.3) amplitudes are highlighted in different colors.

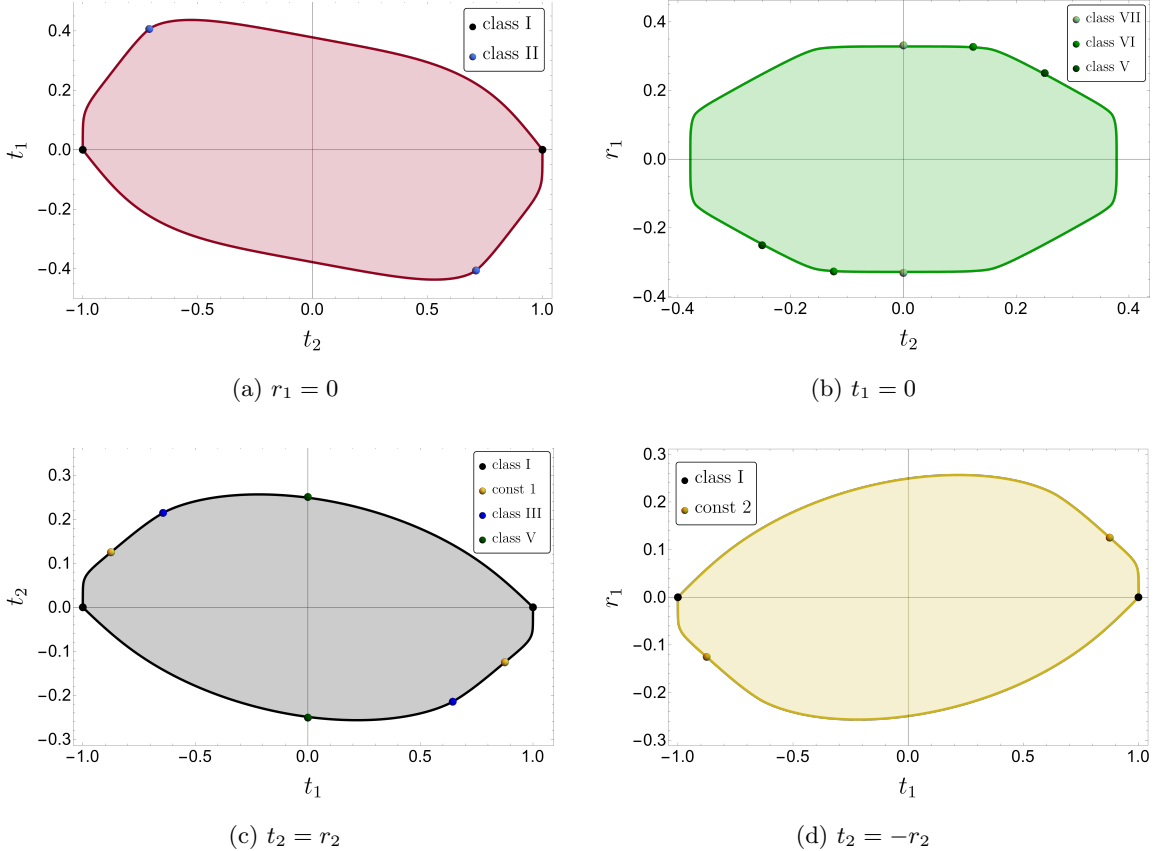


Figure 5: Sections of the $U(7)$ monolith (see solid lines in figure 4), obtained from the dual approach code of appendix C with $n_{max} = 10$, $n_{intpts} = 30$, $precision = 100$ and ~ 1000 angles.

is present in the vast majority of extremal amplitudes with group-like symmetries. More on this point and the possible connection to complex conformal field theories are discussed in the next section.

4 Discussion

In this work we have begun to chart the space of amplitudes with a global $U(N)$ symmetry for massive Quantum Field Theories in two spacetime dimensions. We focused on the two-to-two scattering of particles in the fundamental/antifundamental representation of $U(N)$ without bound states. We observed integrable models emerging at special points of the boundary of the allowed regions. Most of these integrable amplitudes were written down in [11]. Table 1 summarizes the integrable solutions compatible with this symmetry, including two that were missing from the original classification in [11].

The first new solution, labeled $(N=2)_p$ in table 1, can be viewed as a one-parameter deformation of the $O(4)$ nonlinear sigma model and was previously discussed in, e.g., [10, 22, 23]. The second, Class VII in the same table, has no free parameters and represents another Yang-Baxter solution characterized by periodic behavior in real rapidity. To the best of our knowledge, this solution has not previously appeared in the literature.

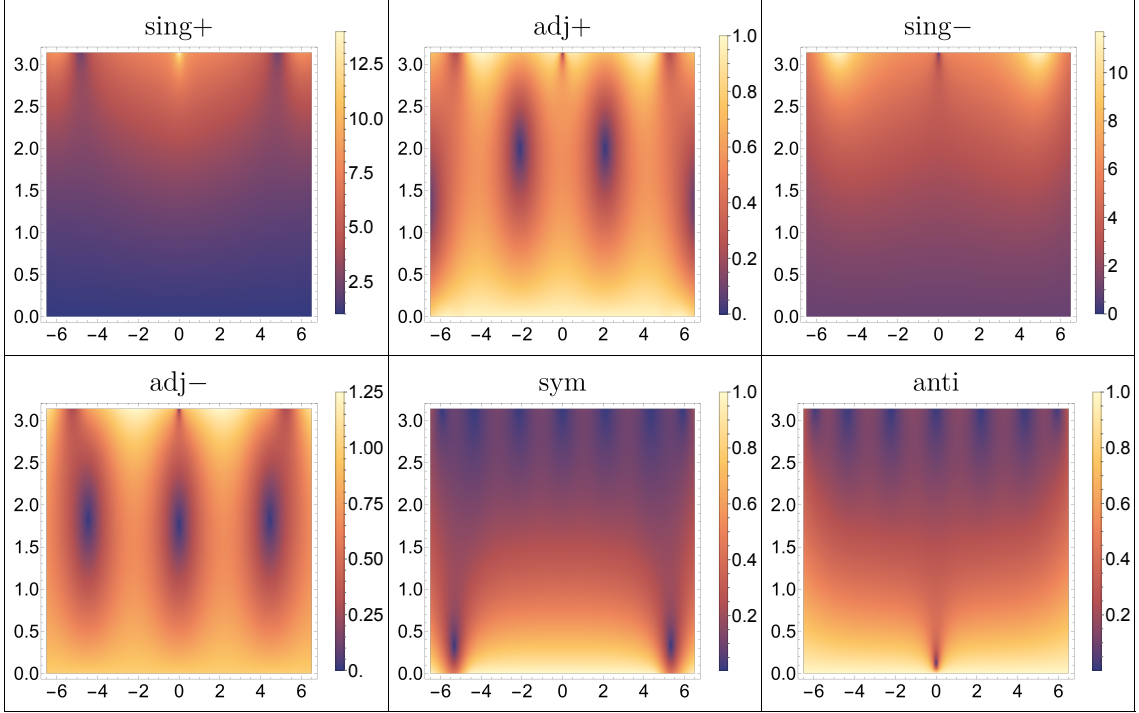


Figure 6: Analytic structure of the amplitudes in the complex θ plane for a generic point on the $U(7)$ monolith close to constant 1 solution (3.3). The plots show an array of zeros signaling resonances in different channels. For these we used the primal bootstrap code with $nmax = 60$, $ngrid=120$.

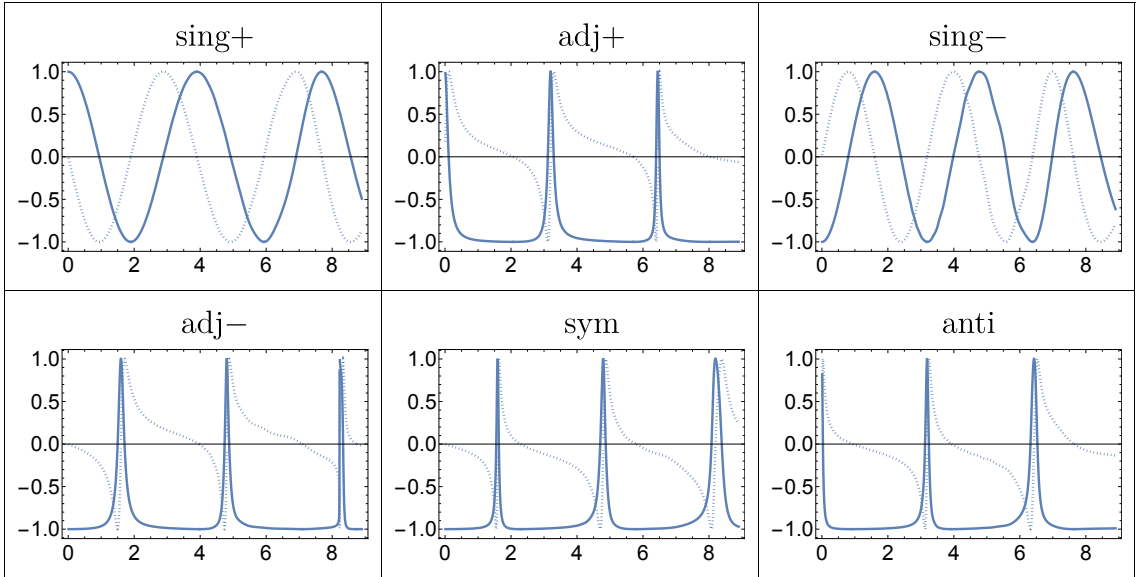


Figure 7: Real (solid) and imaginary (dashed) parts of the amplitudes $S_a(\theta)$ in physical kinematics $\theta \in \mathbb{R}$ for an extremal point close to constant 1 (3.3) with $N = 1000$. These numerical amplitudes show the emergent periodicity present in most of the monolith. To generate these plots with the dual code we used $nmax = 130$, $nintpts = 350$, $precision = 350$.

One of the more puzzling aspects we encountered is the ubiquity of extremal amplitudes with periodic behavior in real rapidity, as has been previously observed for theories with conventional group symmetries [5, 6]. It would be very valuable to understand analytically why the bootstrap optimization problem leads to such space of solutions and why the presence of non-invertible symmetries seems to explore a different space of solutions [8, 31]. While particle production will ultimately break this periodicity, we believe that the amplitudes we found remain a good approximation of the physical ones at low energies.

An exception is given by integrable models where multiparticle processes are factorized into a sequence of $2 \rightarrow 2$ amplitudes and particle production is absent. Classes V-VII in table 1 belong to this category, characterized by both integrability and periodic behavior. Although the physical realizations of these solutions have not been fully established, we expect them to be related to deformations of complex conformal theories. For the $O(N)$ periodic Yang-Baxter solution in [4, 5, 32] such a connection was proposed in [33].

We briefly review their argument here. The conformal theories are given by the continuum limit of critical $O(N)$ loop models [34], which have two (real) fixed points for $-2 \leq N \leq 2$. From the higher temperature fixed point (also called dilute model) there is a massive deformation described by the integrable $O(|N| \leq 2)$ amplitude of Zamolodchikov [35]. As we approach $N = 2$, the two fixed points merge and become complex for $N > 2$. What the authors of [33] observed is that the $O(N)$ periodic Yang-Baxter solution, naturally defined for $N > 2$, describes the expected walking behavior for the RG flow passing between the two complex CFTs. That is, for a large range of energies, quantities such as the central charge look constant. The walking behavior is more prominent for values of N close to the merging point of CFTs, where the complex CFTs are close to the real line.

What we propose here is that the $U(N)$ periodic amplitudes studied in this work should describe similar walking behaviors. We test this with the integrable amplitudes in classes V-VII, where we can easily compute the two-particle contribution to the UV central charge c_2 using the two particle form factors of the trace of the stress tensor Θ as explained in appendix B. The c-sum rule integral reads

$$c_2(\theta_{\max}) = 3 \int_0^{\theta_{\max}} d\theta \frac{|F_2^\Theta(\theta)|^2}{16 \cosh^4 \frac{\theta}{2}}. \quad (4.1)$$

Here we are performing the integral up to some maximum rapidity θ_{\max} to test the walking behavior.⁹ As we show in figure 8a, we find that classes V-VI walk for $N \gtrsim 1$ around $c = 1$.¹⁰ For class V this behavior is expected, as it corresponds to the $O(2N)$ periodic Yang-Baxter solution and for $N = 1$ coincides with the $O(2)$ NLSM for which $c = 1$. The central charge value for class VI is the same as in class V, as the amplitudes and form factors coincide for $N = 1$.

⁹The full central charge is given by an integral over all energies, i.e. $\theta_{\max} \rightarrow \infty$, which often diverges for these extremal amplitudes (see [15] for the $O(N)$ case). What we are showing here is the approximately constant behavior for a large range of energies.

¹⁰We are quoting the values of c_2 for the integrable amplitudes with an overall minus sign with respect to table 1. The ones with a plus sign walk for the same values of N but have larger central charge.

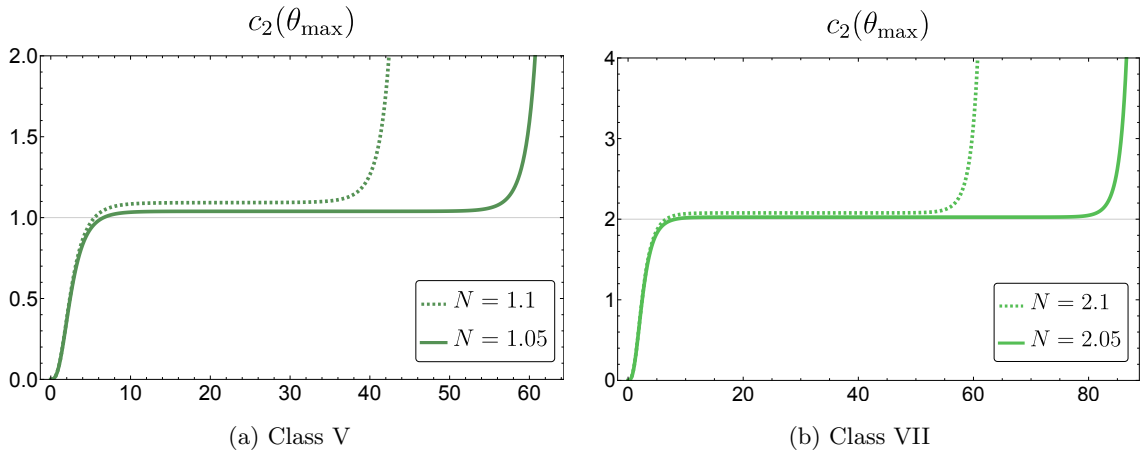


Figure 8: Walking behavior of the central charge for $U(N)$ periodic integrable amplitudes.

Concerning class VII in figure 8b, we see walking behavior for $N \gtrsim 2$ around $c = 2$. A natural question to ask is what is the corresponding UV conformal theory for $N \leq 2$? A candidate theory is given by the critical $U(N)$ loop model studied in [36]. In this model, non-intersecting oriented loops are considered, where all neighboring loops have opposite orientations. Following Zamolodchikov’s logic in [35], we expect the amplitude to contain only the tensor structures associated to $r_{1,2}$ in (2.6), which is indeed the case in class VII. A second hint is that this loop model is conjectured to have the same phase diagram as the $O(N)$ one, so that there is a merging of fixed points at $N = 2$.

There is a discrepancy, however, with the expected central charge at $N = 2$. Our model exhibits walking behavior around $c = 2$ whereas the fixed point studied in [36] has $c = 1$ for this value of N . We should note that the actual symmetry of the model in [36] is $PSU(N)$, since it can be constructed from a spin chain that alternates between fundamental and antifundamental degrees of freedom at each site. With this global symmetry, fundamental excitations are not allowed. In an analogy with the CP^{N-1} model, one expects only meson-like excitations. Nevertheless, if an appropriate term to the CP^{N-1} Lagrangian such as a minimally coupled Dirac fermion with quartic interaction is added, the fundamental excitations become “liberated”. Indeed, this modified model gives rise to the integrable amplitudes of class II and $(N=2)_p$ for a particular choice of parameters [10]. Moreover, since it interpolates between the $O(2N)$ NLSM and $CP^{N-1} +$ free boson, the UV central charge is $c = 2N - 1$ (i.e. one unit larger than for CP^{N-1}). It is possible that a similar mechanism could be at play in the $PSU(N)$ loop models and explain the discrepancy in the central charges. It would be very interesting to understand better this connection, find other loop models with full $U(N)$ global symmetry, and identify a candidate loop model for class VI.

In this work we have added a new piece to the map of two-dimensional QFTs. As with other S-matrix bootstrap studies, generic features of the allowed amplitudes point to interesting behaviors that go beyond conventional expectations. This suggests two paths forward: either formulate new criteria to restrict the space to conventional theories or

embrace the exploration of the novel features. In either case, continued investigation will undoubtedly deepen our understanding of non-perturbative quantum field theory.

Acknowledgements

The authors would like to thank Benjamin Basso, Vasco Gonçalves and Emilio Trevisani for useful discussions. Centro de Física do Porto is partially funded by Fundação para a Ciência e a Tecnologia (FCT) under the grant UID04650-FCUP. R.R. is supported by FCT under the grant 2024.04788.BD, by FCT grant 2024.00230.CERN and HORIZON-MSCA-2023-SE-01-101182937-HeI.

A Solutions to Yang-Baxter equations

In this Appendix we review the different classes of solutions to the Yang-Baxter equations for particles transforming in the fundamental/antifundamental representation of $U(N)$. The first classification was performed in [11], but some solutions were missed there. Here, we present a complete analysis. As stated in [11] there are three¹¹ independent types of Yang-Baxter equations for this case, namely

$$\begin{aligned} S(\theta_{12}) F(\theta_{13}) F(\theta_{23}) &= F(\theta_{23}) F(\theta_{13}) S(\theta_{12}), \\ S(\theta_{12}) F(\theta_{13}) B(\theta_{23}) &= B(\theta_{23}) S(\theta_{13}) F(\theta_{12}) + F(\theta_{23}) F(\theta_{13}) F(\theta_{12}), \\ F(\theta_{12}) S(\theta_{12}) F(\theta_{23}) + B(\theta_{12}) B(\theta_{12}) B(\theta_{23}) &= F(\theta_{23}) S(\theta_{13}) F(\theta_{12}) + B(\theta_{23}) B(\theta_{13}) B(\theta_{12}), \end{aligned} \tag{A.1}$$

each of which encompasses several independent factorization equations. These can be more easily understood by the schematic representation of figure 9.

A simple way to obtain the Yang-Baxter equations is to label the endpoints of the lines in the schematic representations of figure 9 in pairs and then connect them in all possible ways. In each $2 \rightarrow 2$ scattering process, i.e. when two lines intersect, we identify one of the functions u_i, t_i, r_i ($i = 1, 2$) based on the orientation of the arrows. To exemplify this procedure we depict it in a schematic way in figure 10. This should then be repeated for different choices of labeling.

In what follows we will present the equations and respective solutions, which resulted from doing this exercise. We will separate the analysis between general N and $N = 2$, as the latter contains an extra solution with a free parameter.

A.1 General N

Keeping N general and going through the steps mentioned above we get the following set of equations:

$$u_2 t_1 t_2 + u_1 t_2 t_2 = u_2 t_2 t_1, \tag{A.2}$$

$$u_1 t_2 r_2 + u_2 t_1 r_2 = r_1 r_2 t_1, \tag{A.3}$$

$$u_1 t_1 r_2 + u_2 t_2 r_2 = t_1 u_1 r_2 + r_1 r_2 t_2, \tag{A.4}$$

$$t_2 u_1 r_1 + r_2 r_2 t_1 = u_1 t_2 r_1, \tag{A.5}$$

$$t_1 u_2 r_1 + r_1 r_1 t_1 = u_2 t_1 r_1, \tag{A.6}$$

$$u_1 t_1 r_1 = t_1 u_1 r_1, \tag{A.7}$$

$$N t_2 u_2 r_2 + t_1 u_2 r_2 + t_2 u_1 r_2 + t_2 u_2 r_1 + N r_2 r_1 t_2 + r_1 r_1 t_2 + r_2 r_1 t_1 = u_2 t_2 r_1, \tag{A.8}$$

$$\begin{aligned} N t_2 u_2 t_2 + t_2 u_2 t_1 + t_1 u_2 t_2 + t_1 u_2 t_2 + t_2 u_1 t_2 + N r_2 r_1 r_2 + r_2 r_1 r_1 + r_1 r_1 r_2 \\ + r_2 r_2 r_2 = r_1 r_2 r_1, \end{aligned} \tag{A.9}$$

¹¹In [10] the authors write two other kinds of factorization equations stemming from scatterings of the type: $P(\theta_1) P(\theta_2) P(\theta_3) \rightarrow P(\theta_3) P(\theta_2) P(\theta_1)$ and $P(\theta_1) P(\theta_2) A(\theta_3) \rightarrow P(\theta_3) P(\theta_2) A(\theta_1)$. We have checked, however, that the factorization equations coming from these are redundant and as such do not place further constraints which could decrease the number of solutions.

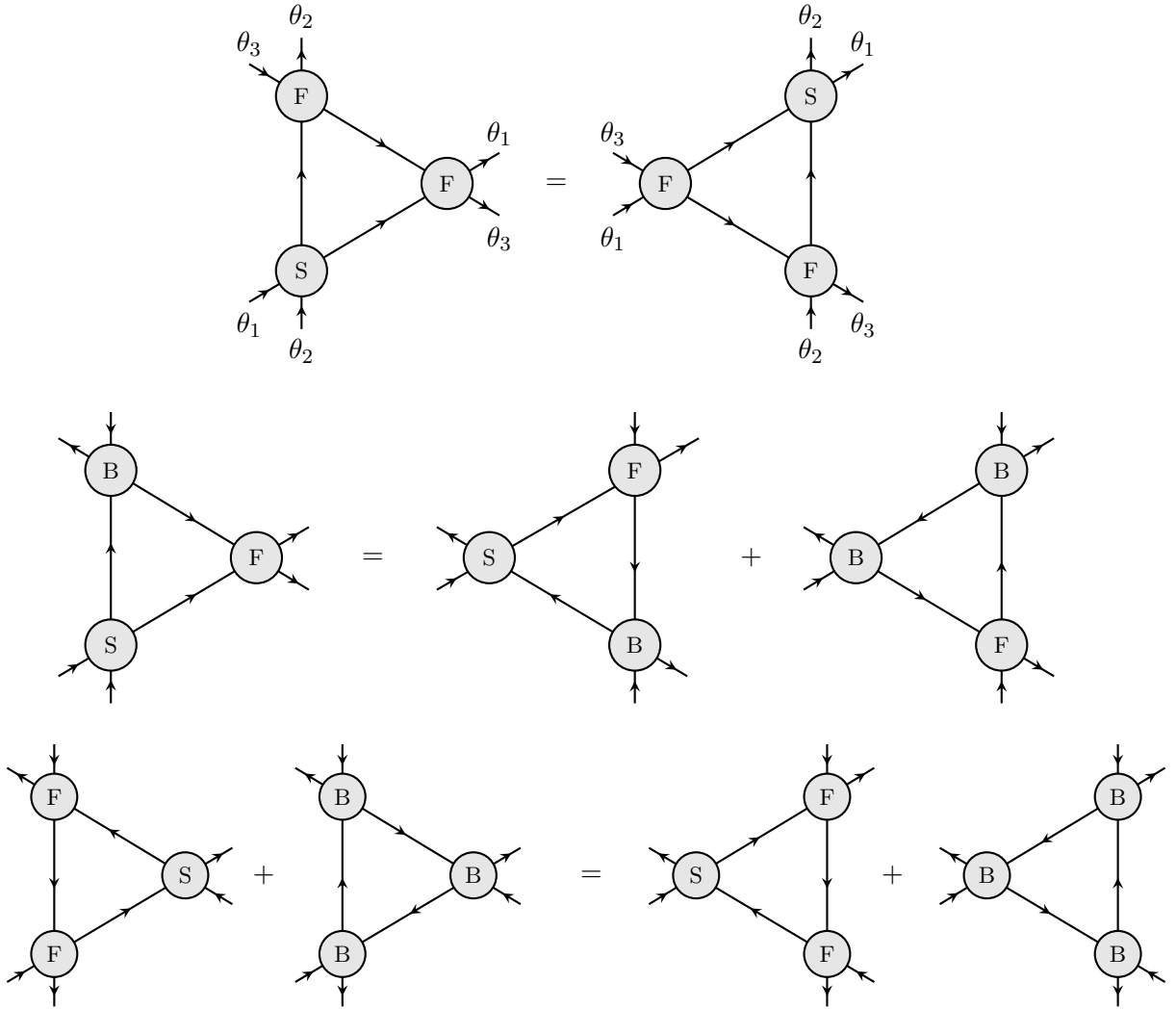


Figure 9: Schematic representation of the three types of Yang-Baxter equations for the case of $U(N)$ scattering. Each line is associated with a given rapidity θ_i , and while arrows oriented upward concern particle states, the ones running downward represent antiparticle states. The $2 \rightarrow 2$ scattering processes are described by the matrices S , F , B defined in (2.4), (2.5) and (2.6).

where in each term the arguments of the functions are θ_{12} , θ_{13} and θ_{23} , respectively. At this point we would like to introduce the variables $\theta = \theta_{12}$ and $\theta' = \theta_{23}$, such that $\theta + \theta' = \theta_{13}$, as these will be used frequently from now on.

In order to solve the above equations and obtain the solutions of table 1 we start by drawing our attention to equation (A.7). It will only hold true if either

$$r_1(\theta) = 0 = r_2(\theta), \quad (\text{A.10})$$

where the second equality comes from crossing, or

$$r_1(\theta) \neq 0 \neq r_2(\theta) \quad \text{and} \quad u_1(\theta) t_1(\theta') = t_1(\theta) u_1(\theta'). \quad (\text{A.11})$$

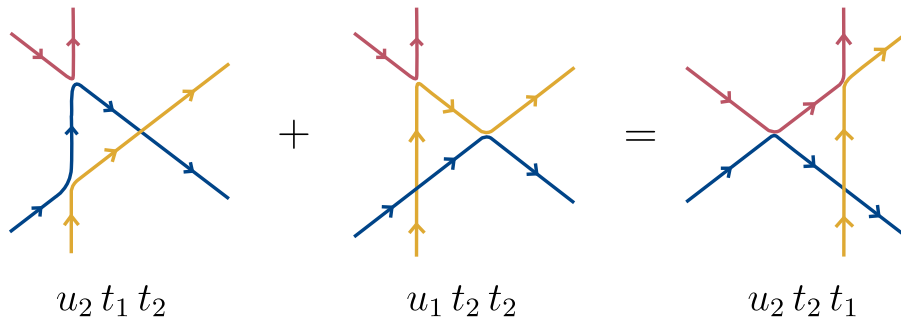


Figure 10: Schematic depiction of the procedure to obtain the Yang-Baxter equations

As such, below we will divide the solutions by whether they satisfy (A.10) or (A.11), starting with the first.

Before this, let us note that there are zero modes in these equations, so that multiplying a given solution by CDD factors¹² gives another integrable amplitude. As usual, we will describe the "minimal solutions" to these equations, given by the set of functions with the minimal amount of zeros and poles. Furthermore, we write the solutions compatible with our no bound states assumption, so that there are no poles in the physical strip.

Class I (Free theory)

The simplest solution to Yang-Baxter equations is the free propagation case. In this scenario, not only is condition (A.10) satisfied as we also have

$$u_2(\theta) = 0 = t_2(\theta), \quad (\text{A.12})$$

such that all equations (A.2-A.9) hold true. The remaining two components are constant and need to satisfy unitarity and crossing. As such they are given by

$$u_1(\theta) = 1 = t_1(\theta). \quad (\text{A.13})$$

Class II

A different solution can be obtained by dropping condition (A.12), implying that $u_2 \neq 0 \neq t_2$, but keeping the assumption (A.10) of no backward scattering. From equation (A.2) we can then use crossing symmetry, $u_1(\theta) = t_1(i\pi - \theta)$, $u_2(\theta) = t_2(i\pi - \theta)$, to write everything in terms of t_1 and t_2 . By defining the function

$$p(\theta) = \frac{t_2(\theta)}{t_1(\theta)}, \quad (\text{A.14})$$

the Yang-Baxter equation (A.2) becomes

$$\frac{1}{p(i\pi - \theta)} - \frac{1}{p(\theta)} + \frac{1}{p(\theta + \theta')} = 0, \quad (\text{A.15})$$

¹²These are functions of the form $\text{CDD}_\lambda(\theta) = \frac{\sinh \theta - i \sin \lambda}{\sinh \theta + i \sin \lambda}$ which are crossing symmetric $\text{CDD}_\lambda(i\pi - \theta) = \text{CDD}_\lambda(\theta)$ and saturate unitarity $\text{CDD}_\lambda(-\theta)\text{CDD}_\lambda(\theta) = 1$.

which admits as solution

$$p(\theta) = \frac{c}{i\pi - \theta}, \quad (\text{A.16})$$

where c is a constant that remains to be determined. Crossing necessarily implies that

$$\frac{u_2(\theta)}{u_1(\theta)} = \frac{c}{\theta}. \quad (\text{A.17})$$

The remaining factorization equations then fix c to be

$$c = -\frac{2i\pi}{N}. \quad (\text{A.18})$$

Upon replacing this solution in the unitarity equations (2.18) we get one nontrivial equation, namely

$$t_1(i\pi - \theta) t_1(i\pi + \theta) = \frac{\theta^2}{\theta^2 + \pi^2 \lambda}, \quad (\text{A.19})$$

where $\lambda = \frac{2}{N}$. As described in [11], one of the defining equations of the function $f_\lambda(\theta)$, already introduced in (3.2), is

$$f_\lambda(i\pi - \theta) f_\lambda(i\pi + \theta) = \frac{\theta^2}{\theta^2 + \pi^2 \lambda}. \quad (\text{A.20})$$

Therefore, for this case, we must have

$$t_1(\theta) = f_\lambda(\theta). \quad (\text{A.21})$$

Classes I and II are the only independent solutions to the Yang-Baxter equations we have found that obey (A.10).

Classes III and IV

We now try to find solutions which satisfy the two conditions in (A.11). In addition to these, we start by assuming that we also have $u_1 \neq 0 \neq t_1$, such that (A.11) implies

$$\frac{u_1(\theta)}{t_1(\theta)} = k, \quad (\text{A.22})$$

with k being a constant to be determined. The above relation simplifies the factorization equations, in particular (A.4), which transforms into

$$u_2 t_2 r_2 = r_1 r_2 t_2. \quad (\text{A.23})$$

One possible solution for this equation is

$$u_2(\theta) = r_1(\theta) \quad , \quad t_2(\theta) = r_2(\theta). \quad (\text{A.24})$$

Thus, we replace this in the Yang-Baxter equations, we use crossing to write everything in terms of r_1 and t_1 and similarly to what was done for class II we define a ratio function

$$\rho(\theta) = \frac{r_1(\theta)}{t_1(\theta)}. \quad (\text{A.25})$$

After doing this, equation (A.6) becomes

$$\frac{1}{\rho(\theta)} + \frac{1}{\rho(\theta')} = \frac{1}{\rho(\theta + \theta')}, \quad (\text{A.26})$$

whose solution is given by

$$\rho(\theta) = \frac{b}{\theta}, \quad (\text{A.27})$$

where b is an arbitrary constant. Combining crossing together with the relation (A.22) we also get that

$$r_2(\theta) = \frac{b \cdot k}{i\pi - \theta} t_1(\theta). \quad (\text{A.28})$$

Once we replace all of the relations obtained so far in the Yang-Baxter equations we get two remaining independent equations coming from (A.2) (and the same equation from (A.3)) and (A.8) (and a similar equation from (A.9)). The first of these tells us that the following condition needs to be satisfied

$$k(k^2 - 1) = 0. \quad (\text{A.29})$$

Given that the solution $k = 0$ is inconsistent with crossing and our assumption that $r_2 \neq 0$, there are only two possible scenarios:

$$k = 1 \quad \text{or} \quad k = -1. \quad (\text{A.30})$$

Class III ($k = 1$)

If we choose $k = 1$ the non-trivial equation coming from (A.8) fixes the constant b to be

$$b = -\frac{i\pi}{N-1}. \quad (\text{A.31})$$

The only thing missing is the function $t_1(\theta)$, in terms of which everything else is written. To obtain this we use the unitarity conditions (2.18) expressed in terms of the components u_i, t_i, r_i ($i = 1, 2$) and use all the results found so far. If we do this, we get

$$t_1(\theta) t_1(-\theta) = \frac{\theta^2}{\theta^2 + \pi^2 \lambda^2}, \quad (\text{A.32})$$

where $\lambda = 1/(N-1)$. Additionally, we get another constraint for $t_1(\theta)$ if we use both crossing between t_1 and u_1 and the fact that they are related by a constant in this case. In particular, we arrive at the condition

$$t_1(i\pi - \theta) = t_1(\theta). \quad (\text{A.33})$$

The constraints (A.32) and (A.33) are simultaneously satisfied if t_1 is given by

$$t_1(\theta) = f_\lambda(\theta) f_\lambda(i\pi - \theta). \quad (\text{A.34})$$

This results from (A.20) and another of the defining equations of $f_\lambda(\theta)$ [11], namely

$$f_\lambda(\theta) f_\lambda(-\theta) = 1. \quad (\text{A.35})$$

Class IV ($k = -1$)

If on the other hand we choose $k = -1$, (A.8) forces b to be

$$b = \frac{i\pi}{N+1}. \quad (\text{A.36})$$

Analogously to the previous case, the unitarity conditions then tell us that the function t_1 must obey

$$t_1(\theta) t_1(-\theta) = \frac{\theta^2}{\theta^2 + \pi\lambda^2}, \quad (\text{A.37})$$

with $\lambda = 1/(N+1)$. In addition, crossing and the relation between t_1 and u_1 imposes that

$$t_1(i\pi - \theta) = -t_1(\theta). \quad (\text{A.38})$$

It is possible to see that

$$t_1(\theta) = f_\lambda(\theta) f_\lambda(i\pi - \theta) i \tanh\left(\frac{\theta - i\frac{\pi}{2}}{2}\right), \quad (\text{A.39})$$

satisfies both constraints (A.37, A.38), with the factor $i \tanh[(\theta - i\frac{\pi}{2})/2]$ in particular taking care of the anti-crossing property (A.38). We point out, however, that it also places a zero¹³ at the crossing-symmetric point $\theta = i\pi/2$.

Class V

Another possibility for (A.11) to hold is by having¹⁴.

$$u_1 = 0 = t_1. \quad (\text{A.40})$$

Setting this in the Yang-Baxter equations we once again conclude that (A.24) needs to be satisfied. After using (A.11) and (A.24) we get one nontrivial equation for the ratio of functions

$$a(\theta) = \frac{r_2(\theta)}{r_1(\theta)}, \quad (\text{A.41})$$

¹³The solution in [11] inserts a pole at $\theta = i\pi/2$. Given that we are not assuming any bound states in the spectrum of the theory, we cannot have such poles. To go from the expression found in [29] to the one found here, we multiply by a CDD factor $\text{CDD}_{\pi/2}(\theta) = \frac{\tanh\frac{1}{2}(\theta - i\pi/2)}{\tanh\frac{1}{2}(\theta + i\pi/2)}$.

¹⁴If one of them is null the other also needs to be by crossing.

coming from (A.8) and (A.9), namely

$$a(\theta) - a(\theta + \theta') + a(\theta') + 2N a(\theta) a(\theta') + a(\theta) a(\theta + \theta') a(\theta') = 0. \quad (\text{A.42})$$

Due to crossing between r_1 and r_2 , $a(\theta)$ must satisfy $a(i\pi - \theta) = 1/a(\theta)$. It can be shown that the general solution to this equation is

$$a(\theta) = \frac{\sin \mu \theta}{\sin \mu (i\pi - \theta)}, \quad (\text{A.43})$$

where μ is fixed by (A.42) to be

$$\cosh(\pi\mu) = N. \quad (\text{A.44})$$

We point out that our solution for $a(\theta)$ in (A.43) is the inverse of the one written for class V in [11]. However, the former is the correct one since poles on the physical strip (outside the imaginary axis for the rapidity) would lead to a causality violation. Moreover, their expression does not satisfy Yang-Baxter equations.

At this point only r_1 remains to be fixed. In order to do this we use the only independent unitarity condition for this case

$$r_1(\theta) r_1(-\theta) = 1, \quad (\text{A.45})$$

which together with (A.43) and crossing leads to

$$r_1(-i\pi + \theta) r_1(-i\pi - \theta) = -\frac{\sin \mu(i\pi - \theta) \sin \mu(i\pi + \theta)}{\sin^2 \mu \theta}. \quad (\text{A.46})$$

Given that the sine function can be expressed as

$$\sin x = \prod_{n=1}^{\infty} \left(1 - \frac{x^2}{\pi^2 n^2}\right), \quad (\text{A.47})$$

one can write (A.46) in such a way that it is relatively simple to make a connection with (A.20) and show that the solution is given by

$$r_1(\theta) = \prod_{k=-\infty}^{\infty} \frac{f_{1-ik/\mu}(\theta)}{f_{ik/\mu}(\theta)}. \quad (\text{A.48})$$

Class VI

To get a different solution we recognize that (A.23) is also satisfied if we have

$$u_2(\theta) = c(\theta) r_1(\theta) \quad , \quad t_2(\theta) = c(i\pi - \theta) r_2(\theta), \quad (\text{A.49})$$

where $c(\theta)$ is an arbitrary function to be determined. The second equation comes from crossing. Using these relations, equation (A.4) requires that $c(\theta)$ obeys

$$c(\theta) c(\theta' - \theta) = c(\theta'), \quad (\text{A.50})$$

which is satisfied by $c(\theta) = e^{i\mu\theta}$, where μ is a (in principle complex) parameter to be determined. However, for this class unitarity demands that $\|u_2(\theta)\|^2 = 1$ and $\|r_1(\theta)\|^2 = 1$, which in turn implies that $\|c(\theta)^2\| = 1$, so that $\mu \in \mathbb{R}$. Similarly to the previous class, r_1 is given by (A.48) and r_2 is related to r_1 by (A.41, A.43). Using all of these relations as input for the Yang-Baxter equations, we arrive at last at

$$e^{\pi\mu} = N, \quad (\text{A.51})$$

stemming from (A.8) and (A.9).

Class VII

Finally, there is another solution not considered in [11] where $u_1 = 0 = t_1$ and $u_2 = 0 = t_2$. Setting r_2 related to r_1 as in class V by (A.43), we get a similar equation that involves r_1 , the only difference being $N \rightarrow N/2$. Consequently, in this case the constant μ gets fixed by (A.9) to be

$$\cosh \pi\mu = \frac{N}{2}. \quad (\text{A.52})$$

Given that the unitarity condition remains unchanged from class V, the function $r_1(\theta)$ has the same form as in (A.48).

A.2 $N=2$

We now turn our attention to the case of $N = 2$. Naturally, all the solutions obtained before are still valid for $N = 2$ but as it turns out this case admits an extra solution, more specifically a family of solutions, characterized by a continuous parameter, which was first derived in [22] (see also [10]).

Repeating the exercise mentioned before to arrive at the Yang-Baxter equations, we obtain the set of independent equations¹⁵

$$u_1 u_2 u_2 + u_2 u_2 u_1 = u_2 u_1 u_2, \quad (\text{A.53})$$

$$u_1 t_2 t_2 + u_2 t_2 t_2 = u_2 t_2 t_2. \quad (\text{A.54})$$

$$u_1 t_1 r_1 + u_2 t_1 r_1 = t_1 u_1 r_1 + t_1 u_2 r_1 + r_1 r_1 t_1, \quad (\text{A.55})$$

$$u_1 r_1 u_1 + u_1 r_1 u_2 + u_2 r_1 u_1 + u_2 r_1 u_2 = t_1 r_1 t_1 + r_1 u_1 r_1 + r_1 u_2 r_1, \quad (\text{A.56})$$

$$u_1 t_1 r_2 + u_2 t_1 r_2 + u_1 t_2 r_2 + u_2 t_2 r_2 = t_1 u_1 r_2 + r_1 r_2 t_1 + r_1 r_2 t_2, \quad (\text{A.57})$$

Starting with the first two equations (A.53) and (A.54), and taking into account the crossing relations between u_i and t_i ($i = 1, 2$), it is simple to see that these admit as solutions

$$u_2(\theta) = \frac{c}{\theta} u_1(\theta) \quad , \quad t_2(\theta) = \frac{c}{i\pi - \theta} t_1(\theta), \quad (\text{A.58})$$

¹⁵We point out that (A.53) and (A.56) do not come from the type of Yang-Baxter equations in figure 9 but rather from the ones we mentioned in the footnote below (A.1). In particular, (A.53) is of the type $SSS = SSS$ while (A.56) corresponds to $SBS = FBF + BSB$, where the order of arguments is θ_{12} , θ_{13} , θ_{23} respectively. We have chosen these equations to match with previous literature [10] and because in this $N = 2$ case they turn out to be more straightforward to solve.

where c is an arbitrary constant.

We now shift our focus to equations (A.55) and (A.56) and re-express them as

$$m(\theta + \theta') + n(\theta) n(\theta') = m(\theta) m(\theta') \quad (\text{A.59})$$

$$n(\theta) m(\theta + \theta') + n(\theta') = m(\theta) n(\theta + \theta'), \quad (\text{A.60})$$

where we have made the following definitions

$$m(\theta) = \frac{u_1(\theta) + u_2(\theta)}{r_1(\theta)}, \quad n(\theta) = \frac{t_1(\theta)}{r_1(\theta)}. \quad (\text{A.61})$$

To give an idea on how to solve (A.59) and (A.60) we follow the logic of appendix A in [29]. Thus, we start by setting either $\theta = 0$ or $\theta' = 0$ from which we find that we must have: $n(0) = 0$, $m(0) = 1$. Next, we differentiate with respect to θ' , for example, and set $\theta' = 0$ afterwards, thus obtaining

$$m'(\theta) + \beta n(\theta) = \alpha m(\theta) \quad (\text{A.62})$$

$$m(\theta) n'(\theta) = n(\theta) m'(\theta) + \beta, \quad (\text{A.63})$$

where the following definitions have been made

$$\alpha = m'(0), \quad \beta = n'(\theta). \quad (\text{A.64})$$

These equations can be transformed into

$$m''(\theta) m(\theta) - m'(\theta)^2 + \beta^2 = 0, \quad (\text{A.65})$$

$$n(\theta) = \frac{\alpha m(\theta) - m'(\theta)}{\beta}. \quad (\text{A.66})$$

In order to solve these we must remember to impose the appropriate boundary conditions: $m(0) = 1$, $m'(0) = \alpha$, $n(0) = 0$, $n'(0) = \beta$. It is possible to see that the solutions for $m(\theta)$ and $n(\theta)$ satisfying both (A.65) and (A.66), and the aforementioned boundary conditions are given by

$$m(\theta) = -i \frac{\sinh\left(\frac{i\pi - \theta}{p}\right)}{\sin\left(\frac{\pi}{p}\right)}, \quad n(\theta) = -i \frac{\sinh\left(\frac{\theta}{p}\right)}{\sin\left(\frac{\pi}{p}\right)}, \quad (\text{A.67})$$

where we have made the following choice of re-parametrization of α and β :

$$\alpha = i \frac{\cot \frac{\pi}{p}}{p}, \quad \beta = -i \frac{\csc \frac{\pi}{p}}{p}, \quad (\text{A.68})$$

in order to simplify the expressions. Indeed, with the above rewriting of these parameters they satisfy the identity

$$\alpha^2 - \beta^2 = \frac{1}{p^2}. \quad (\text{A.69})$$

By making use of what we have found so far, in particular (A.58) and (A.67), the remaining Yang-Baxter equation (A.57) fixes the parameter c to be

$$c = -i\pi. \quad (\text{A.70})$$

The last missing piece is then $u_1(\theta)$. Since all Yang-Baxter equations are solved at this point, we turn to the unitarity condition (2.18), which imposes

$$u_1(\theta) u_1(-\theta) = \frac{\theta^2}{\pi^2 + \theta^2}. \quad (\text{A.71})$$

Interestingly, this is exactly (A.20) for $\lambda = 1$, i.e. one of the defining equations of $f_{\lambda=1}(\theta)$. However, we also need to satisfy crossing between $u_1(\theta)$ and $t_1(\theta)$, which in this case looks like

$$t_1(\theta) = -\frac{\sinh\left(\frac{\theta}{p}\right)}{\sinh\left(\frac{i\pi-\theta}{p}\right)} \left(1 + \frac{\pi}{i\theta}\right) u_1(\theta) = u_1(i\pi - \theta). \quad (\text{A.72})$$

Bearing in mind that $f_1(\theta)$ obeys $f_1(\theta) = -\left(1 + \frac{\pi}{i\theta}\right) f_1(i\pi - \theta)$, one can write the solution to (A.71) as

$$u_1(\theta) = \frac{\theta}{\theta - i\pi} f_1(\theta) \xi_p(\theta), \quad (\text{A.73})$$

where $\xi_p(\theta)$ necessarily needs to satisfy

$$\xi_p(\theta) \xi_p(-\theta) = 1, \quad (\text{A.74})$$

$$\xi_p(i\pi - \theta) = \frac{\sinh\left(\frac{\theta}{p}\right)}{\sinh\left(\frac{i\pi-\theta}{p}\right)} \xi_p(\theta). \quad (\text{A.75})$$

The solution to these equations is well known [29] and can be expressed in an integral representation as (see e.g. section 18.8 of [37])

$$\xi_p(\theta) = -\exp\left[i \int_0^\infty \frac{d\omega}{\omega} \frac{\sinh\left(\frac{\pi\omega(p-1)}{2}\right)}{\sinh\left(\frac{\pi\omega p}{2}\right) \cosh\left(\frac{\pi\omega}{2}\right)}\right]. \quad (\text{A.76})$$

This is the Sine-Gordon soliton scattering phase as mentioned in [10].

The $N = 2$ continuous parameter solution is thus defined by

$$\begin{aligned} u_1(\theta) &= \frac{\theta}{\theta - i\pi} f_1(\theta) \xi_p(\theta) = t_1(i\pi - \theta), \\ u_2(\theta) &= \frac{\pi}{i\theta} u_1(\theta) = t_2(i\pi - \theta), \\ r_1(\theta) &= i \frac{\sinh\left(\frac{\pi}{p}\right)}{\sinh\left(\frac{i\pi-\theta}{p}\right)} \left(1 + \frac{\pi}{i\theta}\right) u_1(\theta) = r_2(i\pi - \theta). \end{aligned} \quad (\text{A.77})$$

It is interesting to note that this family of solutions parametrizes a continuous line on the surface of the $U(2)$ monolith which interpolates between class II ($p \rightarrow 1$) and class III ($p \rightarrow \infty$). Consequently, due to the $S \rightarrow -S$ symmetry we have a similar line of solutions on the other side of the boundary. However, for $p < 1$ the solution has poles inside the physical strip associated with bound states and as such these amplitudes are found outside the monolith.

B Integrable form factors and c-sum rule

Here we briefly review the relation between amplitudes, form factors and central charge used in section 4, for more details see e.g. [15]. The starting point is Zamolodchikov's c-theorem [38] which can be expressed as the following sum rule for the trace of the stress tensor Θ

$$c^{\text{UV}} - c^{\text{IR}} = 12\pi \int_0^\infty ds \frac{\rho_\Theta(s)}{s^2}, \quad (\text{B.1})$$

where ρ_Θ is the spectral density defined as $2\pi \rho_\Theta(s) = \int d^2x e^{-ip \cdot x} \langle \Theta(x) \Theta(0) \rangle$. Since we are dealing with gapped theories, we have $c^{\text{IR}} = 0$ and the sum rule computes directly the UV central charge. By inserting a complete set of states in $\langle \Theta(x) \Theta(0) \rangle$, we can read off the n -particle contribution to the central charge $c = \sum_n c_n$.¹⁶ We will be interested in the two-particle contribution to this sum rule c_2 , since we can compute it from the two-particle amplitudes at hand and associated form factors. The sum rule then becomes

$$c = c_2 + \dots = 3 \int_{4m^2}^\infty ds \frac{|F_\Theta(s)|^2}{s\sqrt{s}\sqrt{s-4m^2}} + \dots, \quad (\text{B.2})$$

where $F_\Theta(s)$ is the two-particle form factor.

If the theory is integrable, we can straightforwardly compute the two-particle form factor using Watson's equation $F(s) = S(s)F^*(s)$ [39].¹⁷ A simple recipe follows from writing the corresponding amplitude with an integral representation of the form (recall θ is the rapidity variable satisfying $s = 4m^2 \cosh^2 \theta/2$)

$$S(\theta) = \exp \left(\int_0^\infty \frac{dt}{t} \mathbb{f}(t) \sinh \frac{t\theta}{i\pi} \right), \quad (\text{B.3})$$

where the function $\mathbb{f}(t)$ can be read off from the zeros and poles of the amplitude as explained in appendix A of [15]. Then a minimal solution to Watson's equation is given by¹⁸

$$F_{\text{min}}(\theta) = \mathcal{N} \exp \left(\int_0^\infty \frac{dt}{t} \frac{\mathbb{f}(t)}{\sinh t} \sin^2 \left[\frac{t(i\pi - \theta)}{2\pi} \right] \right). \quad (\text{B.4})$$

where \mathcal{N} is the normalization.

Going back to our $U(N)$ amplitudes, we now want to use the ingredients above to compute the central charge sum rule up to different energies as in (4.1). The amplitudes we study here are the periodic solutions given by classes V-VII in table 1. In particular, we are interested in the sing+ channel, as the trace of the stress tensor is a singlet of the

¹⁶In absence of bound states the first term in this sum is the two-particle contribution c_2 .

¹⁷It is also possible to bootstrap the n -particle form factors in these theories [40], although their computation is more involved.

¹⁸The full form factor can be expressed as $F(\theta) = \frac{Q(\theta)}{D(\theta)} F_{\text{min}}(\theta)$, where Q and D are polynomials in $\cosh \theta$ (see e.g. [37] for more details). The first one is operator dependent and the latter is fixed by the S-matrix poles. In the examples discussed below $F_{\text{min}}(\theta)$ with a suitable normalization is enough to describe $F_\Theta(\theta)$.

$U(N)$ symmetry with even parity. These are given by

$$S_{\text{sing}+}^{\text{V}}(\theta) = s(\mu_{\text{V}}|\theta), \quad \mu_{\text{V}} = \frac{\text{arccosh } N}{\pi}, \quad (\text{B.5})$$

$$S_{\text{sing}+}^{\text{VI}}(\theta) = e^{-i\mu_{\text{VI}}\theta} s(\mu_{\text{VI}}|\theta), \quad \mu_{\text{VI}} = \frac{\log N}{\pi}, \quad (\text{B.6})$$

$$S_{\text{sing}+}^{\text{VII}}(\theta) = s(\mu_{\text{VII}}|\theta), \quad \mu_{\text{VII}} = \frac{\text{arccosh } N/2}{\pi}, \quad (\text{B.7})$$

where we have defined

$$s(\mu|\theta) = \frac{\sinh \mu (\pi - i\theta)}{\sinh \mu (\pi + i\theta)} \prod_{k \in \mathbb{Z}} F_{\pi + \frac{ik\pi}{\mu}}(-\theta), \quad (\text{B.8})$$

and $F_{\lambda}(\theta)$ is given by a ratio of the building block functions $f_a(\theta)$ in (3.2)

$$F_{\lambda}(\theta) = \frac{f_{\frac{\lambda}{\pi}}(-\theta)}{f_{\frac{\lambda}{\pi}-1}(-\theta)} = \frac{\Gamma(\frac{\lambda+i\theta}{2\pi}) \Gamma(\frac{\lambda-i\theta+\pi}{2\pi})}{\Gamma(\frac{\lambda-i\theta}{2\pi}) \Gamma(\frac{\lambda+i\theta+\pi}{2\pi})}. \quad (\text{B.9})$$

The expression formally coincides with the singlet channel amplitude of the $O(N)$ periodic Yang-Baxter solution and the associated $\mathbb{f}(t)$ and $F_{\text{min}}(\theta)$ were written down in [15]. Using their results, we have:

$$\mathbb{f}_{\text{sing}+}^{\diamond}(\theta) = \mathbb{f}(\mu_{\diamond}|\theta), \quad \text{with } \diamond = \text{V, VI, VII}. \quad (\text{B.10})$$

where we have defined the kernel associated to (B.8)

$$\mathbb{f}(\mu|t) = \frac{4\pi\mu e^{-t}}{1+e^t} \sum_{p=0}^{\infty} \frac{\delta(t-2\pi\mu p)}{1+\delta_{p,0}}. \quad (\text{B.11})$$

Similarly, the minimum form factors are expressed in terms of

$$F_{\text{min}}(\mu|\theta) = \mathcal{N} \times \exp \left[-\frac{(\pi+i\theta)^2 \mu}{4\pi} + \sum_{p=1}^{\infty} \frac{2e^{-2\pi\mu p} \sin^2[(i\pi-\theta)\mu p]}{\sinh(2\pi\mu p) (1+e^{2\pi\mu p}) p} \right], \quad (\text{B.12})$$

with the corresponding μ parameters. The two-particle form factors for Θ then read

$$F_{\Theta}^{\text{V}}(\theta) = F_{\text{min}}(\mu_{\text{V}}|\theta), \quad F_{\Theta}^{\text{VI}}(\theta) = e^{i\mu_{\text{VI}}\theta/2} F_{\text{min}}(\mu_{\text{VI}}|\theta), \quad F_{\Theta}^{\text{VII}}(\theta) = F_{\text{min}}(\mu_{\text{VII}}|\theta), \quad (\text{B.13})$$

with the normalization $\mathcal{N} = -2\sqrt{2N}m^2$, which can be computed as in [14, 15]. Note that the phase in $F_{\Theta}^{\text{VI}}(\theta)$ is irrelevant for the central charge sum rule.

To generate the plots in figure 8, we need to consider the amplitudes in table 1 with an overall minus sign. For the form factor this implies we should multiply by an overall factor $-i \sinh \frac{\theta}{2}$

$$F_{\Theta}^{\diamond}(\theta) \xrightarrow{S^{\circ} \rightarrow -S^{\circ}} -i \sinh \frac{\theta}{2} F_{\Theta}^{\diamond}(\theta), \quad \text{with } \diamond = \text{V, VI, VII}. \quad (\text{B.14})$$

Classes V and VI are different in general but coincide for $N = 1$ as $\mu_{\text{V}}, \mu_{\text{VI}} \rightarrow 0$. This means that the walking behavior of the central charge in class VI is qualitative the same as class V in figure 8a for $N \gtrsim 1$.

C Primal and dual codes

We leave here the `Mathematica` codes for both the primal and dual approaches that were used to generate all the plots in this work. In particular, we write down the parts which do the optimization and return a point on the boundary of the allowed space. To generate the full figures we simply have to run these in different directions and plot the points at the end.

The first step is to set the value of N . Seeing as here we have studied both $O(2)$ and $O(7)$ we either run

```
n = 2 or n = 7;
```

accordingly. We also define the rho variables used in both ansätze (2.19) and (2.22),

```
r[s0_, s_] := (Sqrt[4-s0]-Sqrt[4-s])/(Sqrt[4-s0]+Sqrt[4-s]);
```

and we set the crossing matrix,

```
c={{1/(2n), (-1+n^2)/(2n), -(1/(2 n)), -((-1+n^2)/(2 n)), (1+n)/2, (1-n)/2},
{1/(2n), -(1/(2n)), -(1/(2n)), 1/(2n), 1/2, 1/2},
{-(1/(2n)), -((-1+n^2)/(2n)), 1/(2n), (-1+n^2)/(2n), (1+n)/2, (1-n)/2},
{-(1/(2 n)), 1/(2n), 1/(2n), -(1/(2n)), 1/2, 1/2},
{1/(2n), (-1+n)/(2n), 1/(2n), (-1+n)/(2n), 0, 0},
{-(1/(2n)), (1+n)/(2n), -(1/(2n)), (1+n)/(2n), 0, 0}};
```

After this is done, we can move on to the primal and dual implementations. We shall start with the former.

C.1 Primal

Although we have implemented both the normal and radial approaches (see [5]) to the primal method, we will only write the latter since it was the one we used the most. Throughout all the functions we will define, we shall leave the number of coefficients of the ansatz $nmax$ and the size of the grid of points where we evaluate unitarity $ngrid$ as arguments. This way we may vary them freely in order to obtain the best results in a reasonable amount of time.

We start by constructing the grid of points for $s \geq 4m^2$ where we will impose unitarity

```
chebyshevGrid[n_] [a_, b_] := (a+b)/2 - (b-a)/2 * Table[Cos[(2j-1)/(2n)\[Pi]], {j, 1, n}];
sgrid[NN_] := sgrid[NN] = N[Table[8/(1+Cos[\[Phi]]), {\[Phi],
N[chebyshevGrid[NN][0, \[Pi]]}], 50];
```

Then, we proceed with setting the ansatz for the S-matrix (2.19)

```
Sn[s_, nmax_] := {singP[0], (-singP[0] + n^2 * sym[0] + n(-singM[0] + sym[0])) / (-1 + n^2),
singM[0], -((singM[0] + n(singP[0] - (1+n) sym[0])) / (-1 + n^2)), sym[0],
-((singM[0] + singP[0] - (1 + n) sym[0]) / (-1 + n))} +
Sum[{singP[n], adjP[n], singM[n], adjM[n], sym[n], anti[n]} *
r[2, s]^n + c.{singP[n], adjP[n], singM[n], adjM[n], sym[n], anti[n]} * r[2, 4-s]^n,
{n, 1, nmax}];
```

where it can be observed that we already used crossing to relate some of the components of the constant part. Additionally, we specify the free parameters which will be fixed by maximization of the functional,

```
varsn[nmax_] := Variables[Sn[3.5, nmax]];
```

Next, we evaluate our ansatz in the previously defined grid of points and impose unitarity to hold in every single one of them,

```
unitn[s_, nmax_] := ComplexExpand[Re[#1]]^2 + ComplexExpand[Im[#1]]^2 <= 1 & /@ Sn[s, nmax];
unitarityn[nmax_, ngrid_] := And@@ Flatten[(unitn[#, nmax] &)/@ N[sgrid[ngrid], 500]];
```

All that is left to do is to define the components $t_1(s)$, $t_2(s)$, $r_1(s)$, since we will be plotting in this space

```
t1n[nmax_] := (Sn[2, nmax][[2]] + Sn[2, nmax][[4]])/2;
t2n[nmax_] := (Sn[2, nmax][[1]] - Sn[2, nmax][[2]])/(2*n)
              + (Sn[2, nmax][[3]] - Sn[2, nmax][[4]])/(2*n);
r1n[nmax_] := (Sn[2, nmax][[2]] - Sn[2, nmax][[4]])/2;
```

With everything defined, we are now in position to construct the main function

```
fsolradialn[theta_, phi_, nmax_, ngrid_] := fsolradialn[theta, phi, nmax, ngrid] =
FindMaximum[{R, And[unitarityn[nmax, ngrid], {t1n[nmax], t2n[nmax], r1n[nmax]} ==
R * {Sin[theta] Cos[phi], Sin[theta] Sin[phi], Cos[theta]}]}, varsn[nmax] ~ Join ~ {R},
MaxIterations -> 10000, Method -> "MOSEK"];
```

which returns a point on the monolith's boundary in the direction defined by polar angle θ and azimuthal angle ϕ . By choosing different angles we can generate the allowed regions in the space of the S-matrices.

C.2 Dual

In the dual approach we start in a similar fashion, by defining the ansatz of the dual variable

```
v1 = {0, 1/4, 0, 1/4, 1/4, 1/4}; v2 = {1/(4n), -(1/(4n)), 1/(4n), -(1/(4n)), 1/4, -(1/4)};
v3 = {1/(4n), (-1+n)/(4n), -(1/(4n)), 1/4(-1+1/n), 0, 0};
Kdn[s_, nmax_] := Kdn[s, nmax] = 2/(Sqrt[s] Sqrt[4-s] * (s-2)) *
(a1*v1 + a2*v2 + a3*v3 + Sum[{singP[n], adjP[n], singM[n], adjM[n], sym[n], anti[n]}
*r[2, s]^n + Transpose[c].{singP[n], adjP[n], singM[n], adjM[n], sym[n], anti[n]}
*r[2, 4-s]^n, {n, 1, nmax}]);
varsdualn[nmax_] := Variables[Kdn[3.5, nmax]];
```

where \mathbf{v}_i are, as previously mentioned, eigenvalues of \mathcal{C}^T with eigenvalue 1 and the coefficients a_i determine the direction in the space of the scattering amplitudes where the point will be.

Next, we need to evaluate the integral of (2.23), which we will want to minimize. Here we chose to perform the integration by Chebyshev quadrature, which can be implemented in the following way

```

gridn[nintpts_,precision_]:=Table[N[Cos[j*\[Pi]/(nintpts+1)],precision],
{j,1,nintpts}];
integralsn[nintpts_,precision_]:=integralsn[nintpts,precision]=
2*Table[Expand[Times@@(x-Drop[gridn[nintpts,precision],{k}])/
Times@@(gridn[nintpts,precision][[k]]-Drop[gridn[nintpts,precision],{k}])]
/.x^(m_.)>Boole[EvenQ[m]]/(m+1)//N[#,precision]&,{k,nintpts}];
fn[x_,nmax_]:=(2/\[Pi])*((16(-1+x))/(1+x)^3)*Total@Abs@Kdn[(8(1+x^2))/
(1+x)^2,nmax];
goaln[nmax_,nintpts_,precision_]:=goaln[nmax,nintpts,precision]=((fn[#,nmax]&)
/@gridn[nintpts,precision]//ExpandAll//Chop).integralsn[nintpts,precision];

```

In the above functions we can choose the number of points *nintpts* with which we numerically evaluate the integral and the *precision* of this procedure, which should be big enough. At the end the `goal` function provides us with the integral's expression, which must be minimized. Before that, however, we define an auxiliary function

```

rep[\[Theta]_,\[Phi]_]:=First[Solve[Sin[\[Theta]]Cos[\[Phi]]*a1
+Sin[\[Theta]]Sin[\[Phi]]*a2+Cos[\[Theta]]*a3==1]];

```

which ensures that we are minimizing along the direction specified by the angles θ , ϕ . Finally, we construct the function that minimizes $\mathcal{F}_d[\mathbf{K}(s)]$, namely

```

solnM[theta_,phi_,nmax_,nintpts_,precision_]:=solnM[theta,phi,nmax,nintpts,
precision]=Module[{angsol=rep[theta,phi],var},var=First[Intersection[
{a1,a2,a3},{angsol[[1,1]]}]];FindMinimum[goaln[nmax,nintpts,precision]
/.angsol>DeleteCases[varsdualn[nmax],var],MaxIterations->1000,
Method->"MOSEK"]//ReplacePart[#,2->Sort[Join[#[[2]],{var->angsol[[1,2]]}
/.[#[[2]]}]]]&];

```

which returns a point in the space of scattering amplitudes. Repeating this for several angles we obtain a surface, where everything outside of it is excluded, like the ones in figures 2 and 4. However, we point out that in order to generate such smooth figures this code takes around an hour, in spite of using MOSEK. A rougher, but still reasonable image with less points, can nonetheless be obtained in a few minutes. Increasing the free parameters *nmax*, *nintpts* and *precision* it is possible to check that the obtained surfaces tend to the optimal bounds and converge to surfaces obtained with the primal approach, thus implying a vanishing duality gap.

References

- [1] M.F. Paulos, J. Penedones, J. Toledo, B.C. van Rees and P. Vieira, *The S-matrix bootstrap. Part I: QFT in AdS*, *JHEP* **11** (2017) 133 [[1607.06109](#)].
- [2] M.F. Paulos, J. Penedones, J. Toledo, B.C. van Rees and P. Vieira, *The S-matrix bootstrap II: two dimensional amplitudes*, *JHEP* **11** (2017) 143 [[1607.06110](#)].
- [3] Y. He, A. Irrgang and M. Kruczenski, *A note on the S-matrix bootstrap for the 2d $O(N)$ bosonic model*, *JHEP* **11** (2018) 093 [[1805.02812](#)].
- [4] L. Córdova and P. Vieira, *Adding flavour to the S-matrix bootstrap*, *JHEP* **12** (2018) 063 [[1805.11143](#)].
- [5] L. Córdova, Y. He, M. Kruczenski and P. Vieira, *The $O(N)$ S-matrix Monolith*, *JHEP* **04** (2020) 142 [[1909.06495](#)].
- [6] C. Bercini, M. Fabri, A. Homrich and P. Vieira, *S-matrix bootstrap: Supersymmetry, Z_2 , and Z_4 symmetry*, *Phys. Rev. D* **101** (2020) 045022 [[1909.06453](#)].
- [7] A. Homrich, J.a. Penedones, J. Toledo, B.C. van Rees and P. Vieira, *The S-matrix Bootstrap IV: Multiple Amplitudes*, *JHEP* **11** (2019) 076 [[1905.06905](#)].
- [8] C. Copetti, L. Cordova and S. Komatsu, *S-matrix bootstrap and non-invertible symmetries*, *JHEP* **03** (2025) 204 [[2408.13132](#)].
- [9] M.F. Paulos and Z. Zheng, *Bounding scattering of charged particles in 1 + 1 dimensions*, *JHEP* **05** (2020) 145 [[1805.11429](#)].
- [10] B. Basso and A. Rej, *On the integrability of two-dimensional models with $U(1) \times SU(N)$ symmetry*, *Nucl. Phys. B* **866** (2013) 337 [[1207.0413](#)].
- [11] B. Berg, M. Karowski, P. Weisz and V. Kurak, *Factorized $U(n)$ Symmetric s Matrices in Two-Dimensions*, *Nucl. Phys. B* **134** (1978) 125.
- [12] M. Hogervorst and S. Rychkov, *Radial Coordinates for Conformal Blocks*, *Phys. Rev. D* **87** (2013) 106004 [[1303.1111](#)].
- [13] M.F. Paulos, J. Penedones, J. Toledo, B.C. van Rees and P. Vieira, *The S-matrix bootstrap. Part III: higher dimensional amplitudes*, *JHEP* **12** (2019) 040 [[1708.06765](#)].
- [14] M. Correia, J. Penedones and A. Vuignier, *Injecting the UV into the bootstrap: Ising Field Theory*, *JHEP* **08** (2023) 108 [[2212.03917](#)].
- [15] L. Cordova, M. Correia, A. Georgoudis and A. Vuignier, *The $O(N)$ monolith reloaded: sum rules and Form Factor Bootstrap*, *JHEP* **01** (2024) 093 [[2311.03031](#)].
- [16] A.L. Guerrieri, A. Homrich and P. Vieira, *Dual S-matrix bootstrap. Part I. 2D theory*, *JHEP* **11** (2020) 084 [[2008.02770](#)].
- [17] M. Kruczenski and H. Murali, *The R-matrix bootstrap for the 2d $O(N)$ bosonic model with a boundary*, *JHEP* **04** (2021) 097 [[2012.15576](#)].
- [18] Y. He and M. Kruczenski, *S-matrix bootstrap in 3+1 dimensions: regularization and dual convex problem*, *JHEP* **08** (2021) 125 [[2103.11484](#)].
- [19] A. Guerrieri and A. Sever, *Rigorous Bounds on the Analytic S Matrix*, *Phys. Rev. Lett.* **127** (2021) 251601 [[2106.10257](#)].
- [20] A. Guerrieri, A. Homrich and P. Vieira, *Multiparticle Flux-Tube S-matrix Bootstrap*, *Phys. Rev. Lett.* **134** (2025) 041601 [[2404.10812](#)].

- [21] MOSEK ApS, 2024.
- [22] P.B. Wiegmann, *EXACT SOLUTION OF THE $O(3)$ NONLINEAR SIGMA MODEL*, *Phys. Lett. B* **152** (1985) 209.
- [23] A.M. Polyakov and P.B. Wiegmann, *Theory of Nonabelian Goldstone Bosons*, *Phys. Lett. B* **131** (1983) 121.
- [24] A. D’Adda, P. Di Vecchia and M. Luscher, *Confinement and Chiral Symmetry Breaking in CP^{n-1} Models with Quarks*, *Nucl. Phys. B* **152** (1979) 125.
- [25] E. Abdalla, M.C.B. Abdalla and M. Gomes, *Anomaly Cancellations in the Supersymmetric $CP^{(N-1)}$ Model*, *Phys. Rev. D* **25** (1982) 452.
- [26] E. Abdalla and M. Forger, *Integrable Nonlinear σ Models With Fermions*, *Commun. Math. Phys.* **104** (1986) 123.
- [27] R. Koberle and V. Kurak, *LIBERATION OF $U(N)$ SOLITONS IN THE $CP^{*(N-1)}$ MODEL BY MASSLESS QUARKS*, .
- [28] R. Koberle and V. Kurak, *Deconfinement in the $CP^{(1N)}$ Model by Massless Fermions*, *Phys. Rev. Lett.* **58** (1987) 627.
- [29] A.B. Zamolodchikov and A.B. Zamolodchikov, *Factorized s Matrices in Two-Dimensions as the Exact Solutions of Certain Relativistic Quantum Field Models*, *Annals Phys.* **120** (1979) 253.
- [30] A. Antunes, M.S. Costa and J. Pereira, *Exploring inelasticity in the S -matrix Bootstrap*, *Phys. Lett. B* **846** (2023) 138225 [2301.13219].
- [31] C. Copetti, L. Cordova and S. Komatsu, *Noninvertible Symmetries, Anomalies, and Scattering Amplitudes*, *Phys. Rev. Lett.* **133** (2024) 181601 [2403.04835].
- [32] M. Hortacsu, B. Schroer and H.J. Thun, *A Two-dimensional σ Model With Particle Production*, *Nucl. Phys. B* **154** (1979) 120.
- [33] V. Gorbenko and B. Zan, *Two-dimensional $O(n)$ models and logarithmic CFTs*, *JHEP* **10** (2020) 099 [2005.07708].
- [34] E. Domany, D. Mukamel, B. Nienhuis and A. Schwimmer, *Duality Relations and Equivalences for Models With $O(N)$ and Cubic Symmetry*, *Nucl. Phys. B* **190** (1981) 279.
- [35] A.B. Zamolodchikov, *Exact S matrix associated with selfavoiding polymer problem in two-dimensions*, *Mod. Phys. Lett. A* **6** (1991) 1807.
- [36] P. Roux, J.L. Jacobsen, S. Ribault and H. Saleur, *Critical spin chains and loop models with $PSU(n)$ symmetry*, *SciPost Phys.* **18** (2025) 033 [2404.01935].
- [37] G. Mussardo, *Statistical field theory: an introduction to exactly solved models in statistical physics*, Oxford Univ. Press, New York, NY (2010).
- [38] A.B. Zamolodchikov, *Irreversibility of the Flux of the Renormalization Group in a 2D Field Theory*, *JETP Lett.* **43** (1986) 730.
- [39] K.M. Watson, *Some general relations between the photoproduction and scattering of pi mesons*, *Phys. Rev.* **95** (1954) 228.
- [40] F.A. Smirnov, *Form-factors in completely integrable models of quantum field theory*, vol. 14 (1992).